Modification of layered double hydroxides using first-row transition metals for superior UV-Vis-NIR absorption and the influence of the synthesis method used

Bianca R. Gevers,*[a] Sajid Naseem,[b] Charles J. Sheppard,[c] Andreas Leuteritz,[b] and Frederick J.W.J. Labuschagné[a]

* Corresponding author: bianca.gevers@tuks.co.za

[a] *University of Pretoria, Department of Chemical Engineering, Institute of Applied Materials, Lynnwood Road, 0002, Pretoria, South Africa.*

[b] *Leibniz-Institut für Polymerforschung Dresden e.V., Hohe Straße 6, 01069, Dresden, Germany.*

[c] *University of Johannesburg, Department of Physics, Cr Research Group, Cnr. University and Kingsway Road, Auckland Park, 2092, Johannesburg, South Africa.*

Abstract

Layered double hydroxides (LDHs) with high and tailorable UV-Vis-NIR absorption were prepared through transition metal (TM) modification. The synthesis method used and amount of TM present were found to influence the UV-Vis-NIR absorption intensity, -range, and the optical bandgap.

1 Introduction

LDHs are a class of anionic clays with the general formula $[M_{1-x}^{II}M_x^{III}(OH)_2][X_{x/q}^{q-} \cdot nH_2O]$. Here $[M_{1-x}^{II}M_x^{III}(OH)_2]$ describes the composition of the LDH layers consisting of trivalent (M^{III}) and divalent (M^{II}) metal cations, $[X_{x/q}^{q-} \cdot nH_2O]$ describes the composition of the anionic interlayer, X represents the interlayer anion with charge q, and x is the molar fraction of trivalent cations to total metal cations in the layer structure.[1]

While LDHs find many applications, some of the most interesting properties of these materials include their capability to interact with light, leading to applications as UV-stabilisers in polymers[2], as photocatalysts[3] for applications in water-splitting (hydrogen generation and oxygen evolution)[4–6], CO_2 reduction[5] and pollutant degradation[6], as photoelectrochemical electrodes[4], and in photovoltaics[7]. Because of their structure and composition, these materials are often referred to as semi-conducting materials and have been tested as electrocatalysts[4,8,9], supercapacitors[4,7,9] and sensors[10,11]. Within these fields, LDHs have achieved activity comparable to or better than that achieved by other materials. A large fraction of this success has been attributed to the octahedral coordination of the MO_6 clusters in the layer that allow LDHs to act similarly to doped semiconductors[12], the linking of metal ions and oxygen leading to the formation of oxo-bridges that block electron-hole transfer recombination through a metal-to-metal charge transfer mechanism[13,14], and charge, structural and surface defects that can inhibit charge recombination by serving as trapping sites for electrons, consequently improving electron an hole separation efficiency, reducing recombination rates and allowing for increased transport efficiency of separated electrons and holes through the material[5]. However, there remain shortcomings in the understanding of the material properties on their performance, specifically with respect to composition, surface area, crystal structure and morphology.[3,6]

To make the application of photo-active materials viable for renewable energy applications, interaction with the full (or at least a large part of the) solar spectrum is vital. Design of LDHs capable of absorbing in the ultraviolet (UV) and visible (Vis) range has, thus, been a focus in the field for a long time. Multiple materials have been presented in literature with UV-Vis spectra showing effective optical absorption in this range[5,6]. Interestingly, however, most materials found in literature focus largely on the presence of three specific metals, Zn, Ti and Cr, which, being UV-

absorptive and unless combined with other metals in the layer structure, will lead to the formation of a predominantly UV-absorbing material. But other LDHs have shown potential for photo-active applications. For example, MgAl-based LDHs have been classified as wide-band semiconductors[15], exhibiting UV-absorptivity[16,17]. They have found application in unmodified- and modified form as photocatalysts in dye-degradation, where these properties are of benefit.[18] Other applications have been attempted, such as photocatalytic water-splitting. Here, Xu et al. (2015), found that the oxidation and reduction potential of MgAl-LDH is incorrectly positioned for water-splitting.[17] However, through incorporation of Fe, Parida et al. (2012) could achieve hydrogen production.[19] Unfortunately, besides promising results in the modification of one of the most basic LDHs (MgAl-LDH), no investigation of the effects of a variety TMs on the bandgap and UV-Vis absorption exists. The understanding of this influence is vital, however, considering the wide-spread use of TMs in the modification of LDHs for photo-applications.

Here, the use of divalent TMs (Co, Ni, Cu and Zn) and trivalent TMs (Fe) to modify the metallic layer composition of quintinite-type (2:1 ratio Mg:Al) LDH to achieve effective UV-Vis-NIR (near infrared) absorption is presented. For this, five molar Mg/Al substitution percentages were investigated, these being 0.5%, 1%, 5%, 10% and 25% to elucidate the effects of TM-doping (0.5% and 1%) and metal replacement (5%-25%) in MgAl-LDH on the UV-Vis-NIR absorption and bandgap. The materials were prepared using the most frequently used LDH synthesis method, co-precipitation (CP)[1], specifically with the aim of producing nano-structured LDHs for high light-absorption-capacity. Because LDHs can be prepared using a variety of synthesis methods that can have a significant effect on their material properties[20,21], the effects of synthesis method and morphology, were also considered. Three MgAl-LDHs (TM-free), one unaged and one aged for direct particle size effect comparisons and one using urea hydrolysis (UH) – a commonly used method[1] – were prepared for this purpose. Further, the synthesis of the 5% and 10% substituted MgAl-LDHs was repeated using UH to compare the effect of the synthesis method on UV-Vis-NIR absorption.

2 Results and Discussion

In this study, we found unaged MgAl-LDH prepared using CP to be UV-absorptive with a peak absorption at 350 nm (Figure 1) corresponding to a bandgap of approx. 3.1 eV (Vis light absorption). The nanostructures had a globular platelet structure and comparable morphology.[20] The same material, but aged for 18 h at 65 °C, consisted of partially intertwined platelets and produced a very similar absorption spectrum but with a broadened UV-band (Figure 1) corresponding to a bandgap of 2.6 eV. In contrast, the MgAl-LDH prepared using UH (MgAl-LDHu) did not exhibit any significant UV-absorption (Figure 1). This material consisted of well-defined, large and somewhat intertwined platelets.[21] All three MgAl-LDHs also showed an absorption band in the NIR range starting at 1400 nm. The intensity of this absorption band was significantly reduced comparing CP and UH materials. The absorption spectra obtained

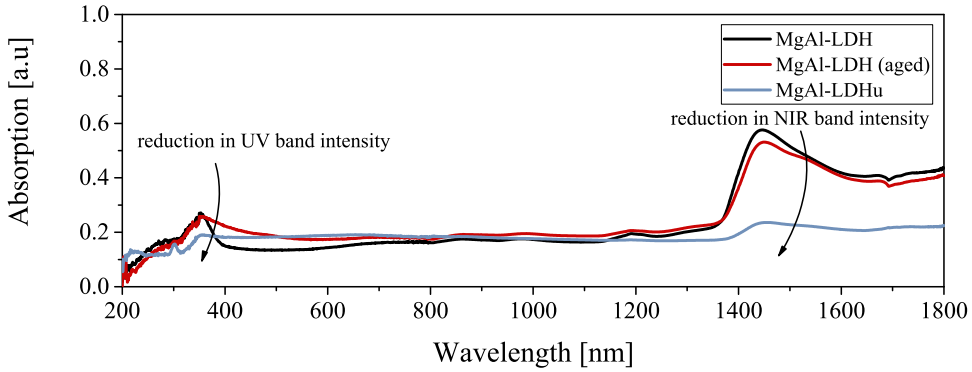

Figure 1 UV-Vis-NIR absorption spectra of MgAl-LDHs prepared using CP, CP with ageing and UH. The spectra show a reduction in the UV and NIR band intensity with an increase in sample crystallinity and platelet size.

for the MgAl-LDHs of this study stand in stark contrast to the those obtained, for example, by Xu et al. (2015), Parida et al. (2012), Carja et al. (2011) and Valente et al. (2009), which showed no absorption or absorption in the UVC, UVB and UVA region.[16,17,19,22] Xu et al. (2015) prepared a MgAl-LDH using a separate nucleation and ageing method leading to the formation of nano-sized, well defined platelets. This MgAl-LDH had a bandgap of 4.18 eV (UVB) and gradually declining UV-absorption from 200 nm – 400 nm with a peak around 225 nm.[17] Parida et al. (2012) prepared

a MgAl-LDH using CP, which lead to the formation of well separated nano-sized platelets, showing a similar absorption spectrum to the MgAl-LDH prepared by Xu et al. (2015) but with a bandgap of 3.5 eV (UVA) and max. absorption at around 210 nm.[19] Carja et al. (2011) prepared a MgAl-LDH using CP that consisted of 100 nm, well separated flakes. This MgAl-LDH showed a similar absorption spectrum to MgAl-LDHu, showing no significant absorption edge in the UV-Vis spectrum.[22] Finally, Valente et al. (2009) prepared a MgAl-LDH using CP. No morphological information was available for this material. This LDH showed absorption at around 200 nm with a bandgap of 5.45 eV (UVC).[16]

Between the materials discussed here, there only exist differences in the synthesis method used – the Mg:Al ratio (2:1) was the same for all. The CP materials prepared in this contribution are unique in having an intertwined nanostructured globular platelet structure with platelet sizes of approx. 170 nm.[20] Upon ageing, this structure was mostly lost, leading to the formation of better crystallised, distinct platelets approx. 230 nm in size, similar to those prepared by other authors. With UH, large, microstructured, somewhat intertwined 2-3 μm diameter platelets were obtained.[21] The effects of platelet size and morphology (typically derived from the synthesis method used) on the interaction of LDHs with light is not yet fully understood, nor is their influence on the materials' electronic structure. To our knowledge, there exists no study constructed specifically for this purpose. Some authors have, however, found a red-shift in the absorption spectra comparing nano-sized and bulk material[23] and that an increase in the surface area of an LDH does not cause a significant change in its absorption spectrum[13]. It has also been found that the bandgap of MgAl-Cl-LDHs is dependent on the cation disordering and layer stacking sequence[15]. In this study we found that variations in crystallinity could also play a role. Because of the three different synthesis methods used (CP, CP (aged) and UH, of which the latter two use heat to induce Ostwald ripening), changes in the MgAl-LDH crystallinity are eminent and were confirmed. The crystallinity followed the order UH $>$ CP (aged) $>$ CP, inversely related to the UV-NIR absorbance (see: Section 5.2).

Upon incorporation of TMs into plain CP MgAl-LDH, we found that doping of the LDH layers with 0.5 mol% and 1 mol% TM led to the loss of the UV-absorption band using Zn, Cu or Co. However, even these small amounts of Fe, Co, Ni or Cu led to the formation of small absorption bands in the UV/UV-Vis range (see Figure 24 in Section 6). Further, the low substitutions seemingly mimicked the UV response of MgAl-LDHu in the reduced presence of the UV absorption band with a peak intensity at 353 nm. However, when, instead of using very small amounts of TM to modify the LDH layers, large amounts of either the divalent or trivalent cation were used, significant changes could be observed in the UV-Vis response for all materials but those modified with Zn (Figure 2). Regardless of the amount of TM-modification, each material exhibited a characteristic absorption band in the NIR spectrum starting at 1400 nm. Apart from MgNiAl-25, the intensity of this absorption band was reduced upon TM-modification. TM-modification of MgAl-LDHu led to the formation of more defined absorption bands in the UV-region and higher absorption intensities in the Vis range, while it led to a reduction in absorbance in the NIR-range (Figure 2). These structures were of much higher crystallinity than those prepared by CP, and it is thus possible that – analogous to the findings by Yan et al. (2010)[15] – the increased absorption could have resulted from an increased cation ordering and more consistent stacking sequence[24,25] – contrasting observations for plain MgAl-LDH. It follows a summary of observations for the modification with each of the TMs. All calculations and relevant figures are given in Section 5.3.

- Fe modification led to increased broad-band absorption of light in the 200 nm to 800 nm range, covering the full UV-Vis spectrum. The bandgap energies could be red-shifted from 3.1 eV for MgAl-LDH to 1.9 eV for MgFeAl-25. A significant band tail was visible for each of the modifications. Upon an increase in Fe-substitution, the fine structure of the absorption spectrum between 300 nm and 600 nm became less evident, albeit with remnants still visible. The materials prepared using UH showed significant increases in light absorption for TM-substitutions of 5 % and 10 %, red-shifting the bandgap to 1.9 eV. Similar reductions of the NIR absorption band intensity were observed for all CP materials. The absorption results obtained significantly out-perform those obtained by Parida et al. (2012) in terms of absorption strength and red-shift for both, the CP and UH materials with much less Fe-substitution than used in their study.[19]
- Co modification also led to increased broad-band absorption of light in the 200 nm to 800 nm range,

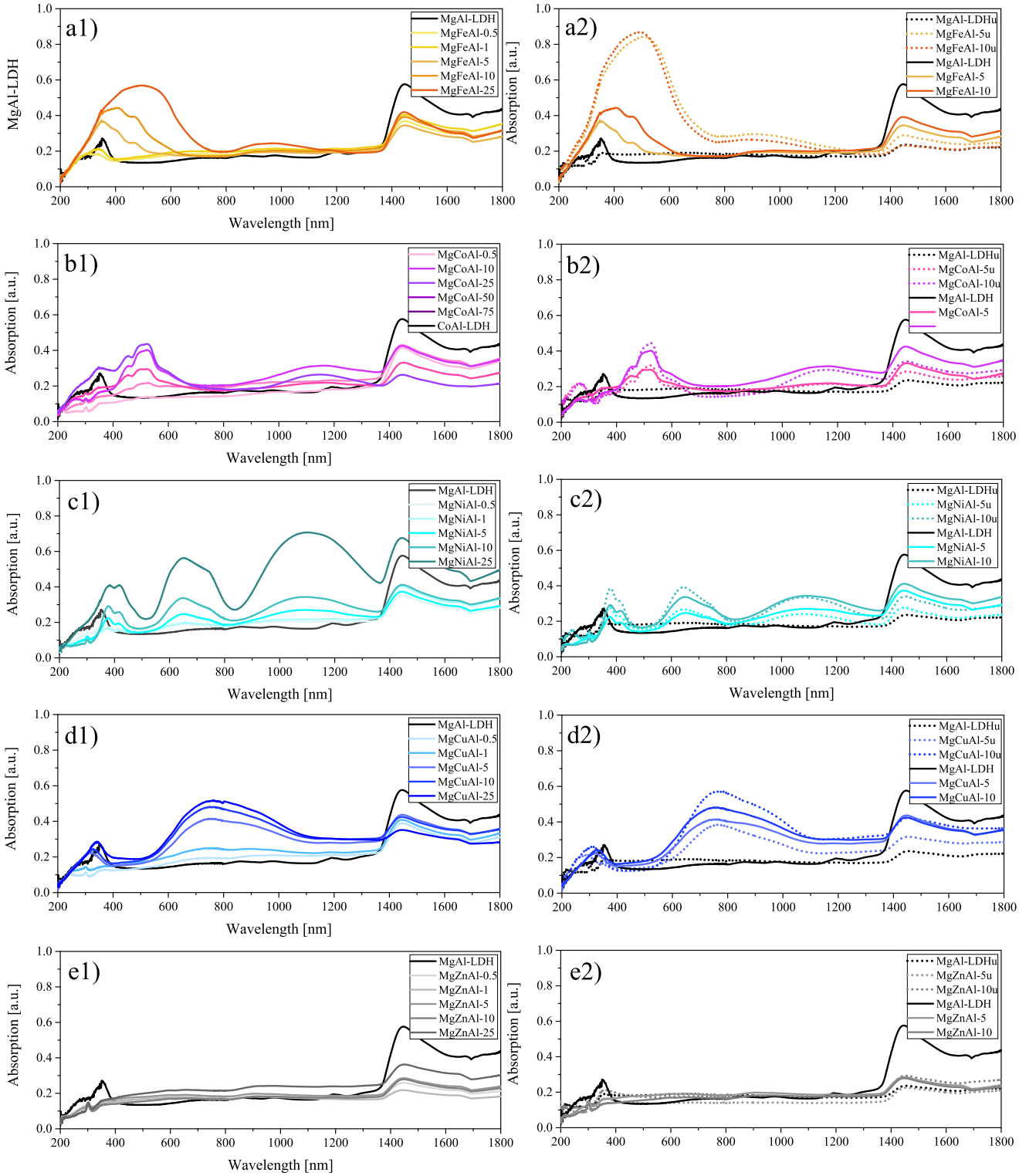

Figure 2 UV-Vis-NIR absorption spectra of 0 %, 0.5 %, 1 %, 5 %, 10 % and 25 % substituted MgAl-LDHs prepared using CP and a comparison of the UV-Vis-NIR spectra for 5 % and 10 % substituted LDHs prepared using UH. a) Fe-substituted b) Co-substituted c) Ni-substituted d) Cu-substituted and e) Zn-substituted MgAl-LDH, (1) prepared using CP and (2) prepared using UH.

covering the full UV-Vis spectrum. The bandgap energies could be red-shifted from 3.1 eV for MgAl-LDH to 2.2 eV, 2.1 eV and 1.7 eV for MgCoAl-25. Again, band tails were visible – but now more so. The Co-modified samples were by far the most complex in terms of their absorption spectra. A significant UV-absorption could only be re-obtained for MgCoAl-25. The materials prepared using UH showed a similar absorption strength and bandgaps for the same TM modifications. However, the UH prepared samples showed a UV-absorption band in the UV B/C region. The NIR absorption band intensity was observed to decrease for 25 % Co modification with respect to MgAl-LDH.

- Ni modification led to increased absorption of light in the 200 nm-500 nm, the 600 nm-800 nm and the 900 nm-1400 nm range, producing three distinct absorption bands with bandgaps of 2.6 eV, 1.5 eV and 0.9 eV. With increasing Ni substitution, the absorption intensity was increased, but the bandgaps remained similar between the 5 %, 10 % and 25 % modifications. The materials prepared using UH showed a similar absorption strength and the same bandgaps for the same TM substitutions. The NIR absorption band intensity increased for 25 % Ni substitution with respect to MgAl-LDH.
- Cu modification led to increased absorption of light in the 200 nm-400 nm and the 600 nm-1100 nm range, producing two distinct absorption bands. Upon Cu-substitution, the bandgaps could be red-shifted from 3.1 eV for MgAl-LDH to 1.0 eV (Vis-NIR band). The materials prepared using UH showed a lower absorption strength for the 5 % modified material and a higher absorption strength for the 10 % modified material. The UH synthesised samples had a broader absorption band in the UV region. The NIR absorption band intensity was decreased for the 5 % Cu-modified UH sample with respect to the other substitution percentages.
- Contrary to the popular usage of Zn-based or Zn-containing LDHs for photo-applications[3–5], the UV absorption band of the MgAl-LDH was severely reduced upon Zn modification for all substitution amounts in the CP samples. In contrast, the samples prepared using UH showed increased UV absorption, albeit small. Zn substitution led to an almost complete removal of the NIR absorption band for low substitution amounts.

The UV-Vis region of an absorption spectrum can indicate potential electronic transitions. Here, however, the substitution of TMs in MgAl-LDH did not produce clean absorption bands with well defined edges required for this. The spectra obtained showed slowly diverging continuous bands (partially overlapping with others) following the peak absorption wavelengths without well-defined coarse and/or fine-structures allowing for indexing of the electronic transition types. This might result from a variety of causes, including defects in the LDH lattice causing electronic structure changes[5], lattice strain presenting as band broadening on the UV-Vis spectrum as a related Urbach energy[26], vibrational-translational effects, intragap levels[5] or the overlapping of multiple absorption bands with different bandgaps. While the study of the impact of defects on LDHs is frequent[5], to our knowledge, no studies exist that target the understanding of UV-Vis-NIR band-broadening for LDHs.

The TMs used in this study form part of the 3d group and differ in the fullness of their d-orbitals. Fe^{3+} has the least filled orbital (d^6), followed by Co^{2+} (d^7), Ni^{2+} (d^8), Cu^{2+} (d^9) and finally Zn^{2+} (d^{10}) which has a fully occupied d-orbital. $d-d$ transitions, therefore, become less likely between the Fe-substituted and Zn-substituted MgAl-LDHs. Typically, $d-d$ transitions are considered forbidden transitions and thus should not contribute to the absorption spectra as significantly as observed here. However, considering the minor absorption capacity of the MgAl-LDHs, we could only link our observations to the inclusion of the TMs into the matrix. Hereby, the ineffectiveness of the Zn-substitution to cause an increase in absorption seems to be consistent with the filled d-orbital not allowing $d-d$ transitions.[17]

As previously mentioned, the LDH matrix consists of octahedrally coordinated MO_6 complexes.[12] These complexes are coordinated through hydrogen bonding to the water and through ionic bonds to the anion in the interlayer. A different charge transfer mechanism could thus be at play – showing its fingerprint in the UV-Vis region. Considering

for this cause ligand field theory and viewing the metal ions as octahedrally coordinated ligand complexes[27,28], it could be possible that the transitions visible are linked to *d*-orbital splitting in presence of a ligand field and that the ionic linkage of the layer to a π orbital rich (carbonate) interlayer region contributes further to this by making available more possibilities for spin distribution across the complicated linkage of $d-$, $p-$ and $s-$orbitals of the atoms present in the structure. Hereby, an increase in the amount of TMs in the layers could lead to a larger overlap area of d-orbitals in the lattice, increasing the options available for electronic transitions and broadening the absorption bands in turn.

Multiple studies have been performed for dimetal LDHs to probe the electronic structure of the material with the aid of density functional theory calculations.[15,17,29] It was found that, in the case of MgAl-LDHs, the conduction band (CB) is populated by unoccupied Mg- and Al-3s and -3p states while the valence band (VB) is populated with O-2p, Mg- and Al-2p states, and anion (in this case Cl)-2p states.[15] Further, the VBs of LDHs were found to be populated by the O-2p orbitals and the TM-3d orbitals incorporated into the LDH layers. The TM-3d orbitals, however, did not only contribute to the VB, but also to the CB, as did the Mg-2p orbital, H-1s orbital and, in some cases, the O-2p orbital (for Ni-containing LDH).[17] While d-orbital splitting might not be the cause of some of the absorption bands observed, considering the "interesting" contribution of the O-2p orbital for Ni-containing LDH as described by Xu et al. (2015)[17], it could, at least in part, be responsible for the vastly-from-literature-differing UV-Vis absorption results observed in this study.

In conclusion, we presented here, to our knowledge, the first findings and comparison of the effects of the kind of TMs and amount of TM substituted in MgAl-LDH on the UV-Vis-NIR absorbance and bandgap of the material as well as results concerning the effects of the synthesis method used. TM-modification could be used to achieve significantly different light absorption behaviour. Clear differences were observed between the absorption spectra obtained for the nanostructured globular platelet-like structures and aged CP materials, and the large platelets prepared using UH. TM-modification for enhanced UV-Vis absorption was successful for Fe-, Co- and Ni-modification, changing the wide-bandgap MgAl-LDH into a narrow bandgap Vis light absorptive material. Cu-modification led to an increased UV-absorption and high-wavelength Vis and NIR absorption. Zn-modification was mostly unsuccessful, contrary to the popular use of these materials in photo-active applications. Finally, comparing UH and CP materials, it could be shown that similar light-interaction behaviours could be recorded regardless of the morphological incongruity of the samples produced with respect to platelet size and dimensions – contrasting the findings for MgAl-LDH. At present, we are in the process of completing deeper investigations into the electronic structure of the materials to fully explain the results.

3 Material synthesis

Six types of MgAl-LDHs were prepared for this study, being unmodified MgAl-LDH and MgAl-LDH modified with Fe, Co, Ni, Cu and Zn LDHs. The materials were prepared using constant co-precipitation (CP) synthesis and urea hydrolysis (UH) according to the method presented by Gevers et al. (2019) and as discussed by Naseem et al. (2019), respectively.[20,21] The samples prepared using constant CP were prepared with molar M^{II+}/M^{III+} ratio of 2:1 and molar substitution percentages (*s*) of 0.5 %, 1 %, 5 %, 10 % and 25 %. The samples prepared using UH were prepared with a molar M^{II+}/M^{III+} ratio of 2:1 and molar substitution percentages (*s*) of 5 % and 10 % for comparative study. Full material characterisation results for the CP samples are presented in Gevers et al. (2019) (X-ray diffraction, scanning electron microscopy, X-ray fluorescence spectroscopy, Fourier-transform infrared analysis, thermogravimetric analysis, particle size analysis) and for the UH samples in Naseem et al. (2019) (X-ray diffraction, scanning electron microscopy - energy-dispersive X-ray spectroscopy, thermogravimetric analysis). A short summary on the synthesis procedure of the CP and UH materials is shown here for the readers convenience. Since the aged MgAl-LDH did not form part of previous studies[20,21], its full synthesis procedure and characterisation is described.

3.1 Co-precipitation

Salt solutions of $MgCl_2 \cdot 6H_2O$ and $AlCl_3 \cdot 6H_2O$ with the correct amounts of Fe, Co, Ni, Cu and Zn salts were prepared by dissolving the metal salts in deionised water. The salt solution was added to a Na_2CO_3 salt solution in a drop-wise fashion while maintaining a pH of 11 ± 0.3 in all experiments through the addition of NaOH solution as required. The

resulting slurry was stirred vigorously throughout the reaction. The precipitated LDH was filtered off using vacuum filtration, washed with 5 L of deionised water, and dried at 60 °C overnight (18 h). The samples were ground to a fine powder after drying. The synthesised LDHs were designated the following naming convention: MgMAl-s with M = Fe, Co, Ni, Cu, Zn and s = 0.5 %, 1 %, 5 %, 10 % and 25 %.

3.2 Aged MgAl-LDH synthesis prepared using CP

Chemically pure $AlCl_3 \cdot 6H_2O$ and $MgCl_2 \cdot 6H_2O$ and analytical grade NaOH and Na_2CO_3 were sourced from ACE Chemicals. Deionised water was used for all experiments. The same method as described for the CP samples was used for the aged MgAl-LDH. However, instead of filtering the sample after synthesis, this sample was stirred continuously at 60 °C for 18 h. The remaining synthesis procedure was followed exactly as described above.

3.3 Urea hydrolysis

Salt solutions of $Mg(NO_3)_2 \cdot 6H_2O$ and $Al(NO_3)_3 \cdot 9H_2O$ with the required amounts of Fe, Co, Ni, Cu and Zn salts were prepared in distilled water, mixed in a round bottom flask, and heated to 100 °C, at which temperature they were maintained for 48 h. The resulting slurry was then cooled down, filtered and washed with distilled water. The filter cake was dried in an oven at 70 °C for 24 h. The synthesized LDHs were designated the following naming convention: MgMAl-su with M = Fe, Co, Ni, Cu, Zn and s = 5 % and 10 %.

4 Material characterisation

4.1 MgAl-LDH (aged)

The aged MgAl-LDH was characterised using X-ray diffraction (XRD), scanning electron microscopy (SEM) and attenuated total reflectance – Fourier-transform infrared (ATR-FTIR) analysis.

XRD measurements were performed on a Panalytical X'Pert PRO X-ray diffractometer in $\theta - \theta$ configuration, equipped with Fe-filtered Co-Kα radiation (1.789 Å) and an X'Celerator detector and variable-divergence- and fixed receiving slits. Samples were prepared according the standardised Panalytical backloading system, which facilitates the nearly random distribution of the particles. Data were collected in the angular range $5^\circ \leq 2\theta \leq 80^\circ$, with a step size of 0.008° 2θ and a 13 s scan step time. The phases were identified using X'Pert HighScore Plus software. The spectra were converted from variable slit to fixed slit prior to phase identification.

SEM images were taken with a Zeiss Gemini 2 Crossbeam 540 FEG SEM (MgAl-LDH and MgAl-LDH (aged)) and a Zeiss Ultra Plus (MgAl-LDHu). The samples were prepared by evenly distributing the samples on carbon tape on an aluminium stub and coating it with two layers of carbon (angles: 0°, -45° and +45°) using a sputter coater. The samples analysed using the Zeiss Ultra Plus were distributed on a stub and sputter coated with 3nm of platinum. The micrographs were taken at 1 keV (4 keV, Zeiss Ultra Plus).

ATR-FTIR spectra were obtained using a Perkin Elmer 100 Spectrophotometer. Samples were pressed in place with a force arm. Spectra were obtained in the range of 550 - 4000 cm^{-1} each with 32 scans at a resolution of 2 cm^{-1}.

4.2 All materials

All materials were analysed using UV-Vis-NIR absorption spectroscopy to obtain the absorption spectra of the materials. UV-Vis-NIR spectroscopy was carried out using an Agilent Technologies Cary 6000i UV-Vis-NIR Spectrophotometer with a DRA-1800 (diffuse reflectance) attachment. The scans were recorded using a 5 mm slit width and an integration time of 0.2 s. The pellets for UV-Vis characterisation were prepared by mixing KBr with the LDHs (70 % KBr and 30 %LDHs) and grinding the mixture for 60 s. The powder was then pressed into pellet form using a pellet press with a pressure of 8 t that was applied for 2 min. The final pellet weighed 300 mg and was 1 mm thick.

5 Supporting Results

5.1 Differences in CP and UH materials

A series of comparable LDHs was prepared using CP. The samples were prepared with morphological similarity and similar platelet sizes. The only differences in material properties of the materials synthesised could be related to the

TMs substituted into the MgAl-LDH.[20] For the UH materials, there were significant differences in the platelet size and also agglomeration. However, they had similar intertwining.

5.2 Material characterisation results comparing MgAl-LDH, MgAl-LDH (aged) and MgAl-LDHu

XRD, shown in Figure 3 a), revealed that the aged MgAl-LDH (like the un-aged MgAl-LDH and MgAl-LDHu) showed clear peaks for the (003), (006), (009), (110) and (115) reflections, as expected for an LDH in the rhombohedral R-3$\bar{m}$ space group and for synthetic quintinite in the rhombohedral (3R) stacking sequence prepared at near-ambient conditions.[30] The ageing led to narrower reflections with higher intensity, linked to a higher sample crystallinity as expected for aged LDHs. No impurity reflections were visible.

In Figure 3 b) the FTIR-ATR spectra for MgAl-LDH, MgAl-LDH (aged) and MgAl-LDHu are shown. Similar results were obtained. The band at 3388 cm^{-1} corresponds to the OH-stretching vibration, and those at 3029 cm^{-1} and 3148 cm^{-1} to the stretching vibrations of water units.[31] The vibrational band at 1600 cm^{-1} corresponds to water-bending[32] of molecules associated to the interlayer anion and was observed between 1630 cm^{-1} and 1586 cm^{-1}. Finally, the characteristic vibrational modes for interlayer CO_3^{2-} are visible around 1012, 870, 1365/1400 and 667 cm^{-1} corresponding to the ν_1, ν_2, ν_3 and ν_4 modes respectively.[33] The remaining vibrations could be assigned to Al–OH translation ($\approx$ 550 cm^{-1} and $\approx$ 759 cm^{-1}), and Al–OH deformation ($\approx$ 930 cm^{-1}).[33]

The crystallite sizes of the MgAl-LDHs (for MgAl-LDH and MgAl-LDH (aged)) were calculated using the Scherrer equation: $\tau = \frac{K\lambda}{\beta cos\theta}$. This formula can be applied for crystallites between approximately 100 nm and 200 nm in size.[34] In this equation τ is the crystallite size (units dependent of those of λ), K is a shape factor (here used as 0.89[35]), λ is the X-ray wavelength used (here 1.78897 Å for Co-Kα radiation), β is the full width at half maximum (FWHM) in radians and θ is the Bragg angle in radians. Using the Scherrer equation, the crystallite sizes of MgAl-LDH and MgAl-LDH (aged) were determined to be 170 nm and 230 nm, respectively.

SEM was used to visually observe these grain sizes and estimate the crystallite size of MgAl-LDHu. The calculated crystallite sizes matched for MgAl-LDH, but were difficult to identify for MgAl-LDH (aged). MgAl-LDHu had crystallites 2-3 μm in diameter. The morphology of the three samples was observed to be different. MgAl-LDH showed globular intertwined platelet structures, while these were mostly removed in MgAl-LDH (aged), which showed smaller, more separated platelets. MgAl-LDHu consisted of partially intertwined platelets that were much better defined and larger.

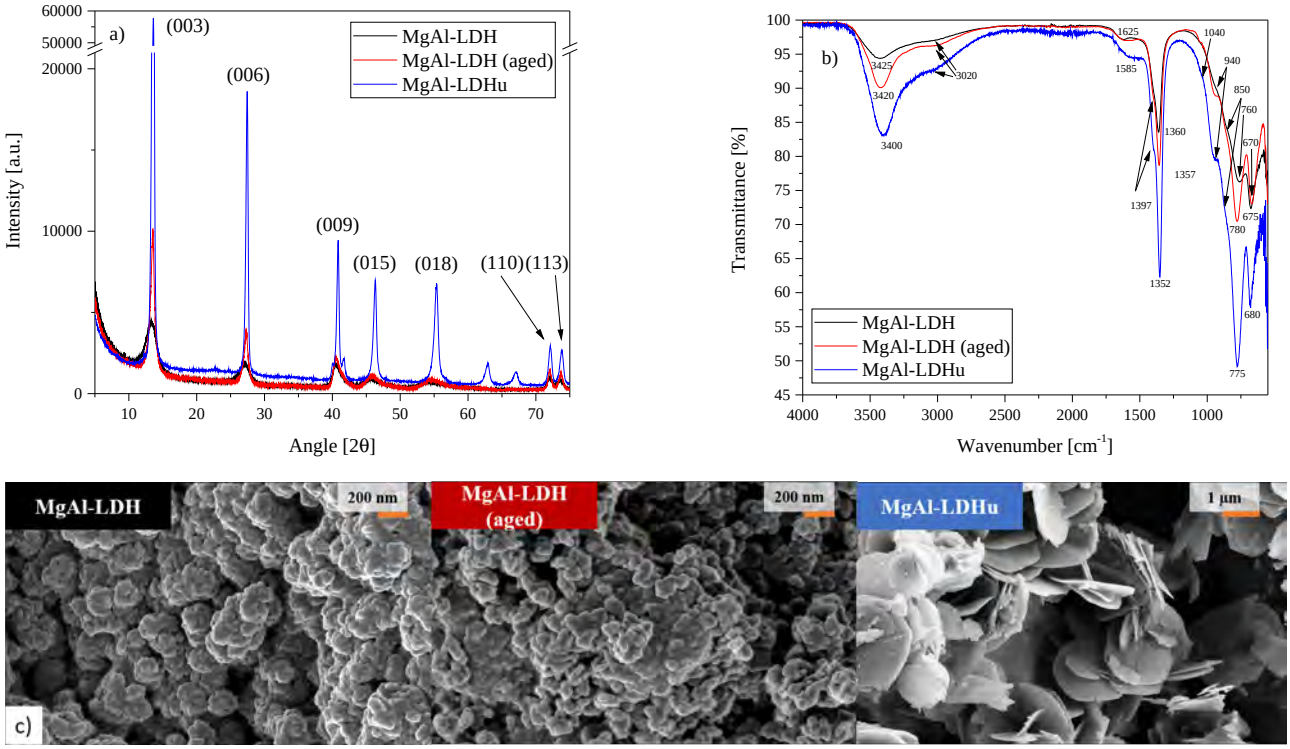

Figure 3 a) XRD b) FTIR-ATR and c) SEM results comparing the results for MgAl-LDH, aged MgAl-LDH and MgAl-LDHu. The orange bar indicates the scale.

5.3 Bandgap determination

The cut-off wavelength (CoW) method and Tauc plot method are the most frequently used in literature to estimate the optical bandgaps of LDHs. Following these most widely used methods, the bandgaps of the materials were estimated using the CoW from absorption spectra[36] and the Tauc plot method[37,38]. For the CoW method, bandgaps were determined by fitting tangent lines to the absorption spectra and horizontal lines to the closest inflection point/minimum. The x-coordinate of the intersection of these two lines, as described in ref [9], was taken as the bandgap of the material. For the Tauc plot method, $(\alpha h\nu)^{1/r}$ is plotted *vs.* $h\nu$, the light energy.[37] As an approximation for α, the absorption coefficient, the Kubelka-Munk function[39–41], $F(R_\infty) = \frac{(1-R_\infty)^2}{2R_\infty}$, was used, where R_∞ is the diffuse reflectance obtained for each sample. r is the type of electronic transition in the material and can have the values 1/2, 3/2, 2 and 3 for direct allowed, direct forbidden, indirect allowed and indirect forbidden transitions.[42] A tangent line is then fitted to the linear region of the resulting plot and the x-axis intercept taken as the bandgap. However, the Tauc plot method only works for materials that are amorphous, nanostructured, and/or (mixed-phase) poly-crystalline materials.[38] The materials prepared here only fit this description for the nanostructured materials prepared using CP.

When Tauc plots are used in literature to estimate the bandgaps of semiconducting materials, the electronic transition types are either known or the materials well studied so that they can be assumed. In addition, these materials frequently show clean absorption edges, so that the Tauc plot method or even the CoW method are easily applied. The absorption spectra obtained for the materials considered in this study mostly did not portray clean absorption edges – in contrast, they portrayed multiple absorption peaks (both, well-defined and/or overlapping). This complicates the application of the Tauc plot and CoW method. Further, we found that typical assumptions of LDHs acting as direct bandgap (allowed transitions)[17,43–45] materials failed to corroborate the bandgaps obtained using Tauc plots and the CoW method for most of the samples. The bandgaps estimated using the Tauc plot method in some cases significantly deviated from those obtained through the CoW method. Methods to determine the electronic transition type as suggested by Sangiorgi et al. (2017) for use in the Tauc plot method failed.[46]

While complex absorption spectra for LDHs have been observed in the past[19,22,43,45], few have made attempts at explaining deviations from clean absorption edges. Any attempts we could find, were explanations based on citations related to other materials rather than characterisation. Currently, we believe that the complex absorption spectra could have resulted from defects in the LDH lattice causing electronic structure changes[5], lattice strain presenting as band

broadening on the UV-Vis spectrum as a related Urbach energy[26], vibrational-translational effects, intragap levels[5] and different types of intra- and interband transitions as observed in other materials[47,48], or the overlapping of multiple absorption bands with different bandgaps. Maybe even phenomena such as (surface) plasmon resonance could be at play as entertained by Carja et al. (2011)[22]. Unfortunately, for LDHs, no systematic studies exist that investigate the effect of these phenomena on their band structure. While analogies to other materials can offer potential explanations, these could also be falsely made. This makes identification of the primary transitions and other effects difficult, if not impossible, at present.

In order to gain some clarity at least on the confidence of the estimated bandgaps using either method, two related methods were used: the absorption spectrum fitting (ASF)[49] procedure (for comparison to the CoW results) and the method used in Zanatta (2019) (use of the complete absorption coefficient (CAC), typically used for thin films and solids)[38] (for comparison to the Tauc plot results). The ASF method makes use only of the absorption data, while the CAC makes use of reflectance and transmission data and requires an electronic transition type. For the ASF method, the Abs/λ is plotted against $1/\lambda$. A tangent line is fitted to the linear region of the spectrum and the intersection with the x-axis taken as the bandgap value.[49] In the CAC method, the complete absorption coefficient is calculated according to $\alpha = +\frac{1}{d} ln \left[\frac{(1-R)^2}{2T} + \sqrt{\frac{(1-R)^4}{4T^2}} + R^2 \right]$, where d is the thickness of the sample, R the reflectance and T the transmittance.[38] $\alpha^{1/r}$ is then plotted against $h\nu$ and similar to the Tauc plot and ASF method, a tangent line fitted to the linear region of the plot and the x-axis intercept taken as the bandgap.

Using these two methods, similar bandgaps to those obtained through the CoW method were obtained using the ASF method. However, completely different bandgaps were obtained using the CAC (some being negative, which is an impossible bandgap value). It is currently being investigated what transition type and potentially multiple transition types the materials have, since none of the methods requiring transition types could produce bandgap values that compared to each other and to the bandgaps determined using the absorbance data. Studies also need to be done on the origin of the band-broadening observed in the absorption spectra to determine its effects and determine the bandgaps more accurately.

Figure 4, Figure 5 and Figure 6 show the bandgaps estimated for MgAl-LDH, MgAl-LDH (aged) and MgAl-LDHu, respectively using the four methods mentioned. Comparing Figure 4, Figure 5 and Figure 6, similar bandgaps were estimated using the CoW, ASF and Tauc plot method, while the CAC yielded impossible results. The CAC was thus not used in any further comparisons. In Figure 7, the bandgaps estimated for MgNiAl-25 using the CoW, ASF and Tauc plot method are shown. Using this more complex spectrum, it was observed that the values for the CoW method and the ASF method were identical, but that the bandgaps determined using the Tauc plot method were significantly higher in this case.

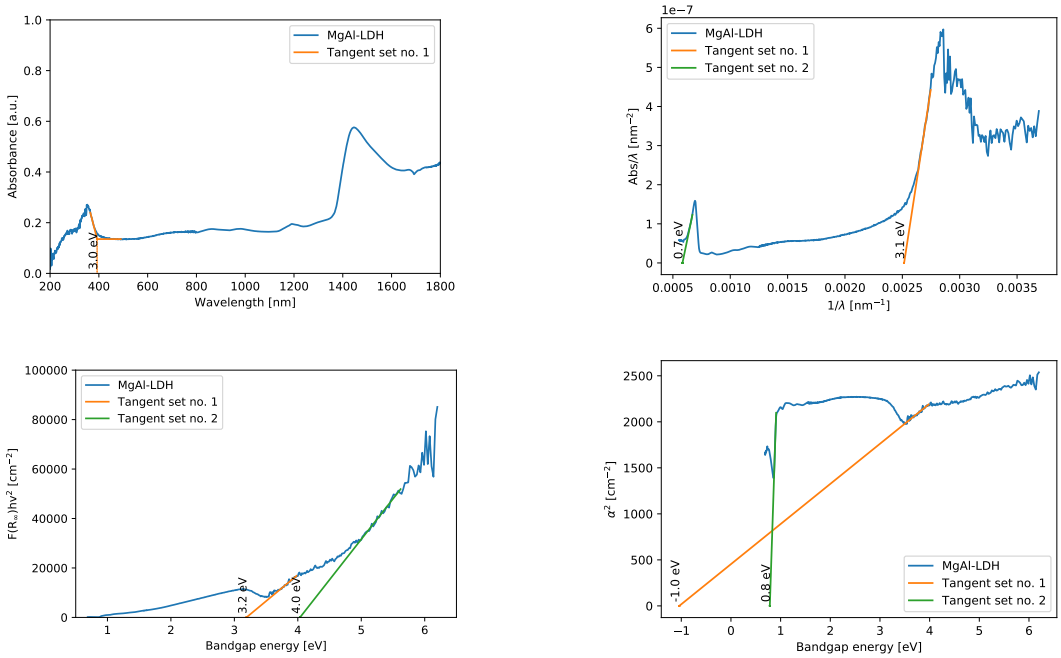

Figure 4 Comparison of the bandgaps obtained for MgAl-LDH using the CoW[36], ASF[49], Tauc plot[37] and CAC[38] method.

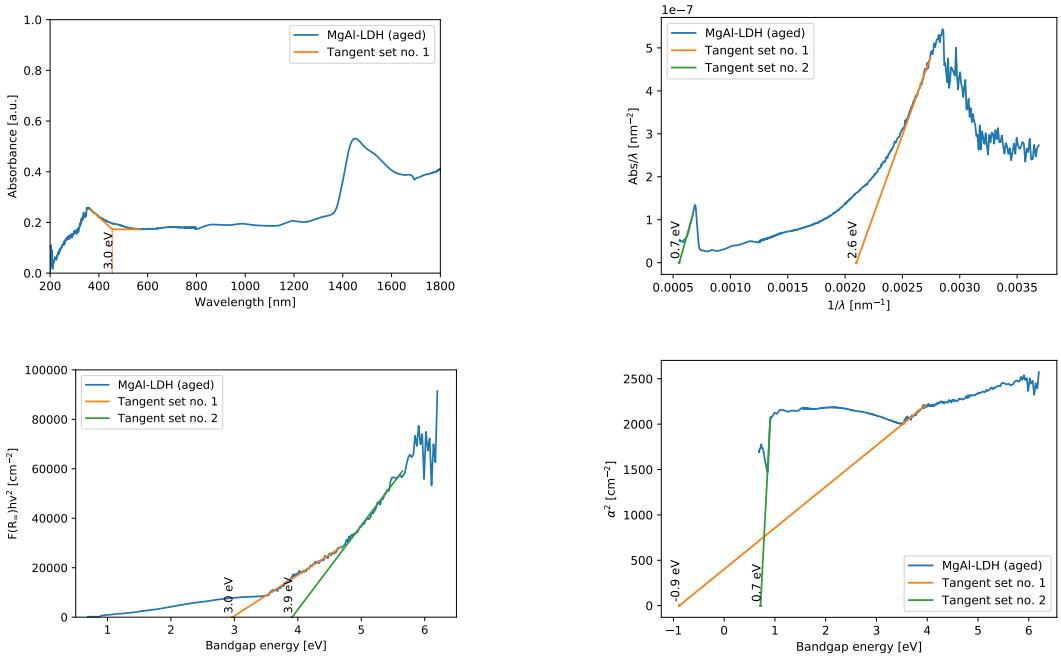

Figure 5 Comparison of the bandgaps obtained for MgAl-LDH (aged) using the CoW[36], ASF[49], Tauc plot[37] and CAC[38] method.

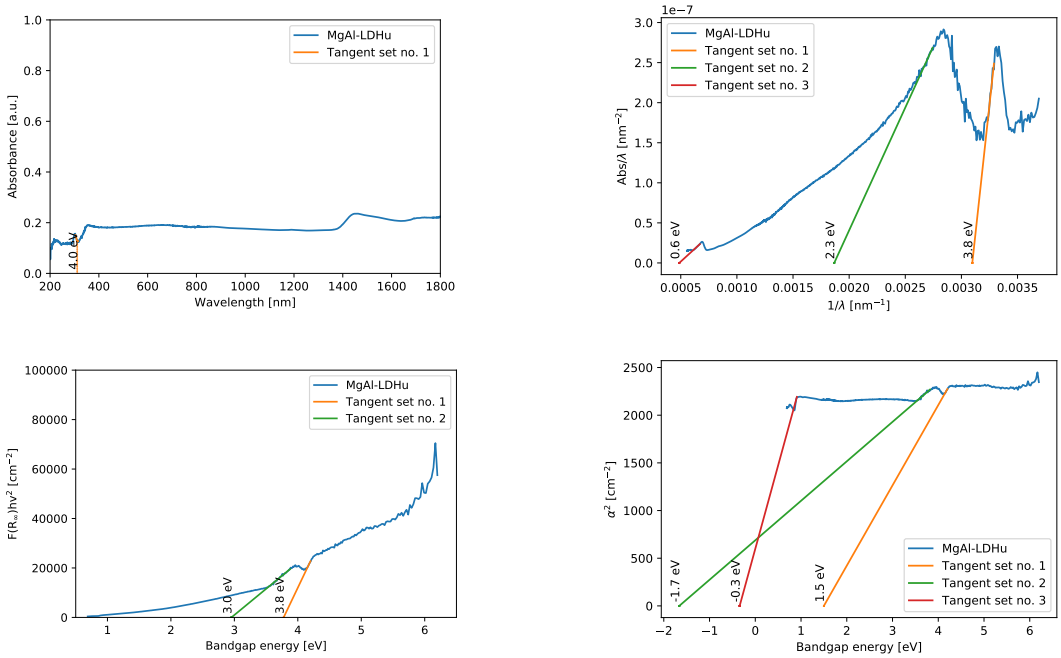

Figure 6 Comparison of the bandgaps obtained for MgAl-LDHu using the CoW[36], ASF[49], Tauc plot[37] and CAC[38] method.

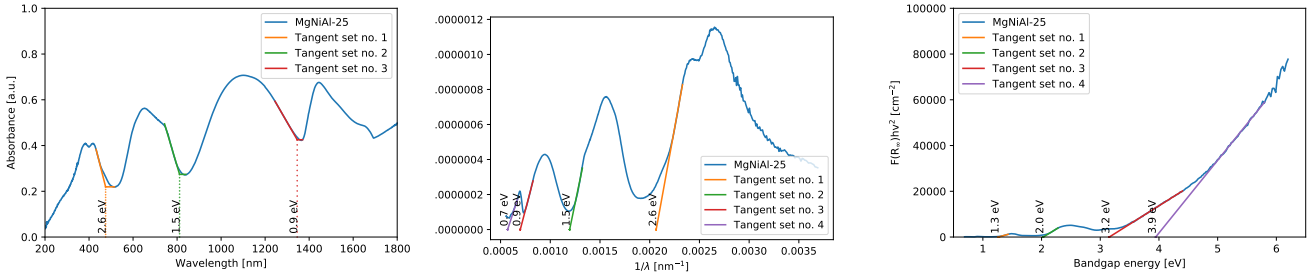

Figure 7 Comparison of the bandgaps obtained for MgAl-LDHu using the CoW[36], ASF[49], Tauc plot[37] method.

It was observed that the ASF method provides higher resolution with respect to the smaller absorption bumps than the CoW method, and because, at this stage, the types of transitions observed in the synthesized LDH materials of this study are unknown, the ASF method was used for further bandgap determinations in this contribution. Results for all three methods are, however, still shown below. The bandgap results for the Fe-, Co-, Ni-, Cu- and Zn-substituted LDHs respectively using the ASF method are shown in Figure 8, Figure 9, Figure 10, Figure 11 and Figure 12. The bandgap results for the Fe-, Co-, Ni-, Cu- and Zn-substituted LDHs respectively using the CoW method are shown in Figure 13, Figure 14, Figure 15, Figure 16 and Figure 17. The results for the Fe-, Co-, Ni-, Cu- and Zn-substituted LDHs respectively using the Tauc plot method are shown in Figure 18, Figure 19, Figure 20, Figure 21 and Figure 22. Finally, the bandgaps determined using the ASF method for the Fe-, Co-, Ni-, Cu- and Zn-substituted LDHs respectively prepared using UH are shown in Figure 23. The figures are shown in the following sections, subdivided into the respective methods used. Table 1 on the following page summarises the bandgaps and band edges observed using the ASF method for all materials in the UVA, Vis and NIR range. No bandgaps in the UVB and UVC region were observed for any of the materials synthesised. The bandgaps were rounded to 2 significant digits to account for inaccuracies in the tangent line fitting process. As visible in Table 1, even small amounts of TM were sufficient to significantly influence the presence of additional absorption bands. However, as will be evident from the figures following, small amounts of TM-modification were not enough to obtain significant enhancement in light absorption.

Table 1 Bandgaps of all materials (MgAl-LDH, MgAl-LDH (aged), MgAl-LDHu and the TM-modified MgAl-LDHs prepared using CP and UH with Fe, Co, Ni, Cu and Zn modification (0.5%, 1%, 5%, 10% and 25% (CP) and 5% and 10% (UH))).

	Bandgap in eV		
	UVA	Vis	NIR
	315-380 nm (3.94-3.26 eV)	380-740nm (3.26-1.68 eV)	740-1800 nm (1.68-0.69 eV)
MgAl-LDH		3.1	0.7
MgAl-LDH (aged)		2.6	0.7
MgAl-LDHu	3.8	2.3	0.6
MgFeAl-0.5		2.9	0.9, 0.7
MgFeAl-1		3	0.9, 0.7
MgFeAl-5		2.6, 2.5, 2.2	0.7
MgFeAl-5u		1.9	
MgFeAl-10		2.3, 2.2	0.7
MgFeAl-10u		1.9	
MgFeAl-25		1.9	0.7
MgCoAl-0.5	3.9		1.6, 0.8, 0.7
MgCoAl-1	3.8	1.8, 1.0	0.7
MgCoAl-5	3.5	2	1.5, 0.7
MgCoAl-5u	3.9	2.1, 1.7	0.7
MgCoAl-10	3.7	2.1, 1.7	0.7
MgCoAl-10u	3.8	2.2, 1.8	0.8, 0.7
MgCoAl-25		2.2, 2.1, 1.7	0.8, 0.7
MgNiAl-0.5	3.9	2.6, 1.9	1.1, 0.7
MgNiAl-1	3.6	2.7, 2.3	1.1, 0.7
MgNiAl-5	3.9	2.9, 2.6,	1.3, 0.8, 0.7
MgNiAl-5u	3.6	2.8, 2.6	1.4, 0.8, 0.7
MgNiAl-10	3.9	2.8, 2.6	1.4, 0.8, 0.7
MgNiAl-10u	3.8	2.9, 2.7	1.5, 0.9, 0.7
MgNiAl-25		2.6	1.5, 0.9, 0.7
MgCuAl-0.5		2.5	0.8, 0.7
MgCuAl-1		2.4	1.1, 0.9, 0.7
MgCuAl-5		3	1.1, 1.0, 0.7
MgCuAl-5u	3.3	2.9	1.2, 0.6
MgCuAl-10		3	1.0, 0.7
MgCuAl-10u		3.2	1.1, 0.6
MgCuAl-25		3	1.0, 0.7
MgZnAl-0.5	3.7	1.9	1.0, 0.7
MgZnAl-1	3.7		1.1, 0.7
MgZnAl-5	3.7		1.1, 0.8, 0.7
MgZnAl-5u	3.9	2.3	0.6
MgZnAl-10	3.8		1.0, 0.7
MgZnAl-10u	3.9	2.3	0.6
MgZnAl-25	3.9		1.0, 0.7

5.3.1 ASF Method

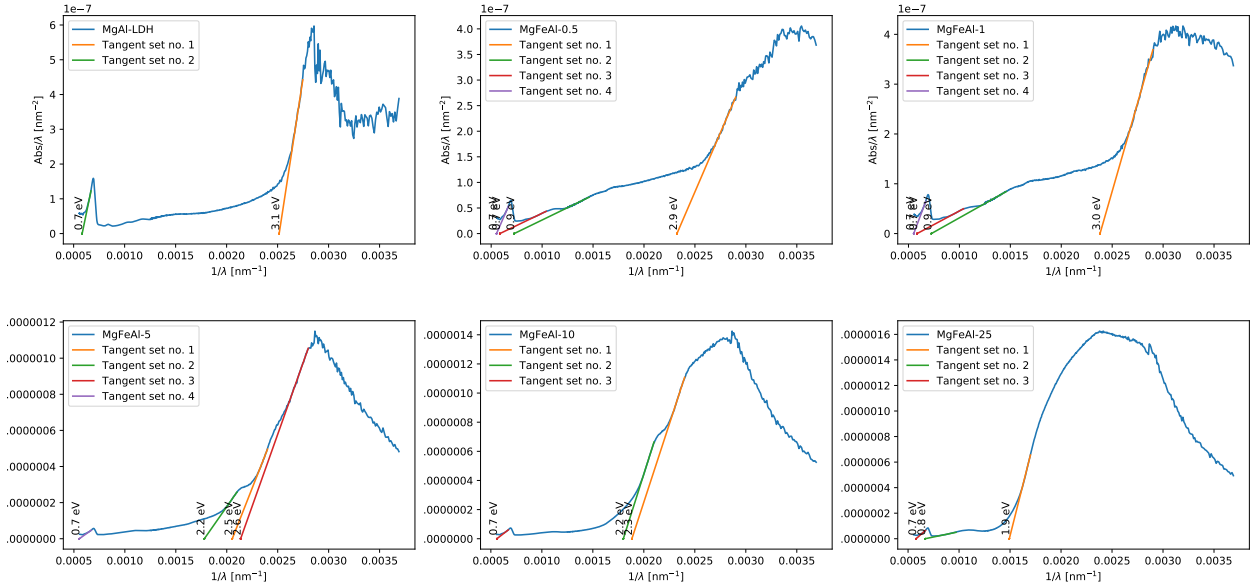

Figure 8 ASF method fitted bandgaps of MgAl-LDH (top left) and the Fe-substituted (0.5, 1, 5, 10, 25% middle left to bottom right) LDHs prepared using CP.

For Fe-substitution, an increase in Fe-content led to a decrease in the bandgap from 3.1 eV to 1.9 eV for 25% substitution. In between, multiple band-edges were also visible. The typical NIR absorption band with a bandgap of 0.7 eV was retained throughout.

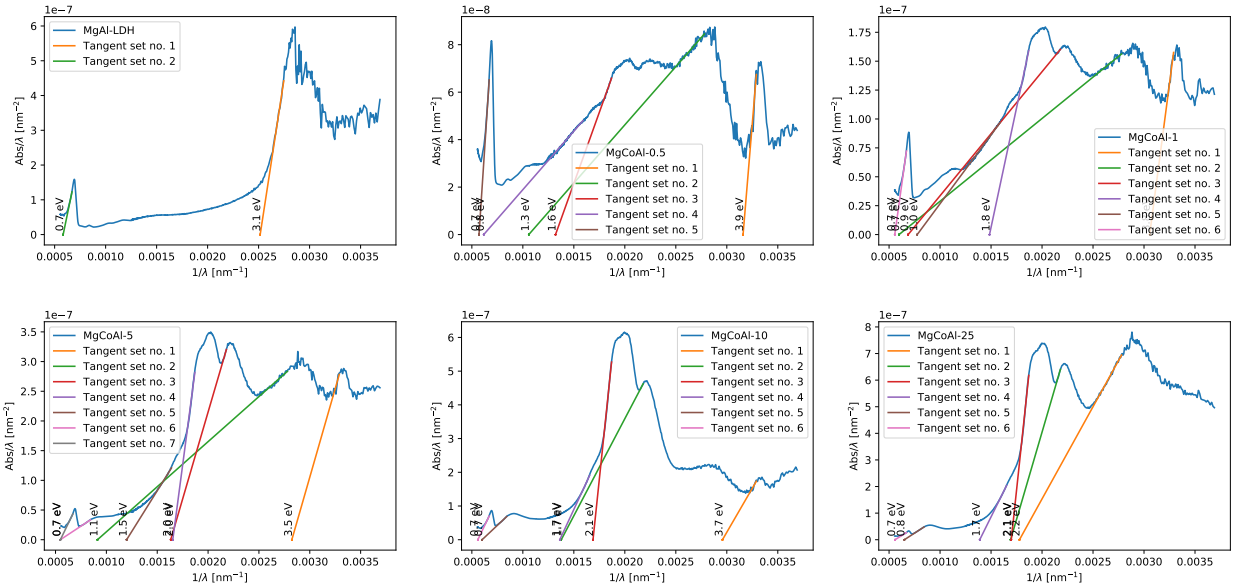

Figure 9 ASF method fitted bandgaps of MgAl-LDH (top left) and the Co-substituted (0.5, 1, 5, 10, 25% middle left to bottom right) LDHs prepared using CP.

For Co-substitution, doping the MgAl-LDH with 0.5% and 1% of Co led to multiple band edges appearing indicating very low bandgaps. These were not taken into account when reporting bandgaps for the materials, as the light absorbency was very low. Bandgaps (for these and all other materials) were also not taken into account when the tangent lines crossed other, lower bandgap tangent lines. Substitution with Co, changed the MgAl-LDH from a 3.1 eV bandgap material to a 2.2, 2.1 and 1.7 eV bandgap material upon modification with 25% Co. The typical NIR absorption band with a bandgap of 0.7 eV was retained throughout.

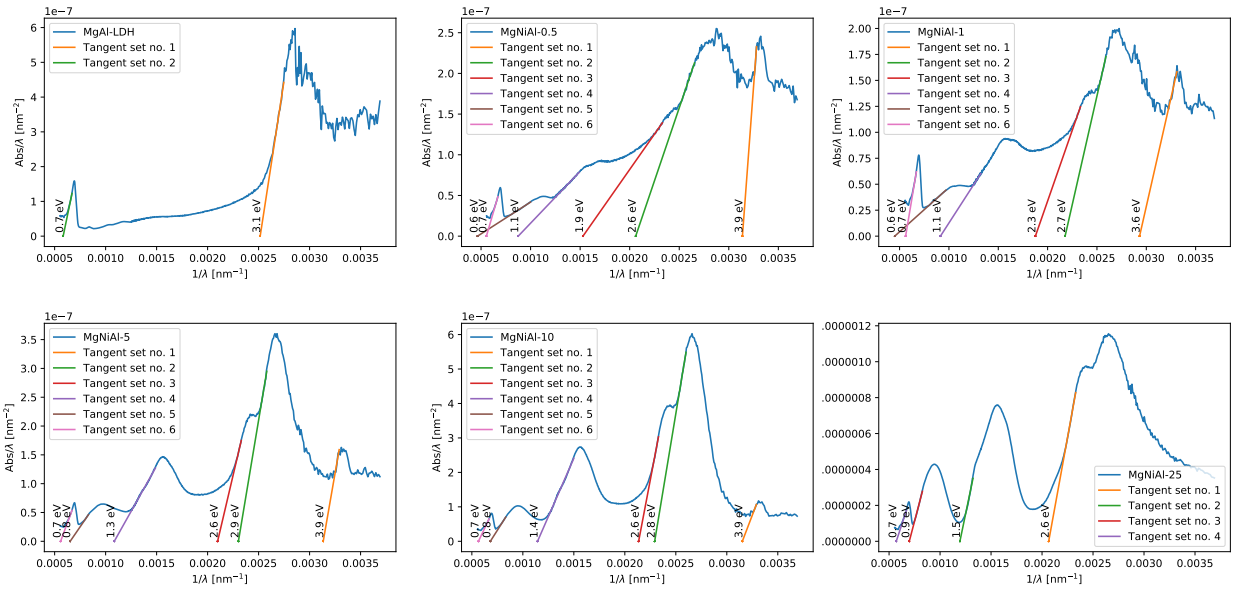

Figure 10 ASF method fitted bandgaps of MgAl-LDH (top left) and the Ni-substituted (0.5, 1, 5, 10, 25% middle left to bottom right) LDHs prepared using CP.

Ni-substitution led to the formation of very distinct absorption bands rather than multiple strongly overlapping ones. Hereby, substitution of 25% Ni led to the formation of three bands with a bandgap of 2.6 eV, 1.5 eV and 0.9 eV in addition to the typical 0.7 eV bandgap that every LDH exhibited. Well defined bands were only visible from 5% Ni-substitution.

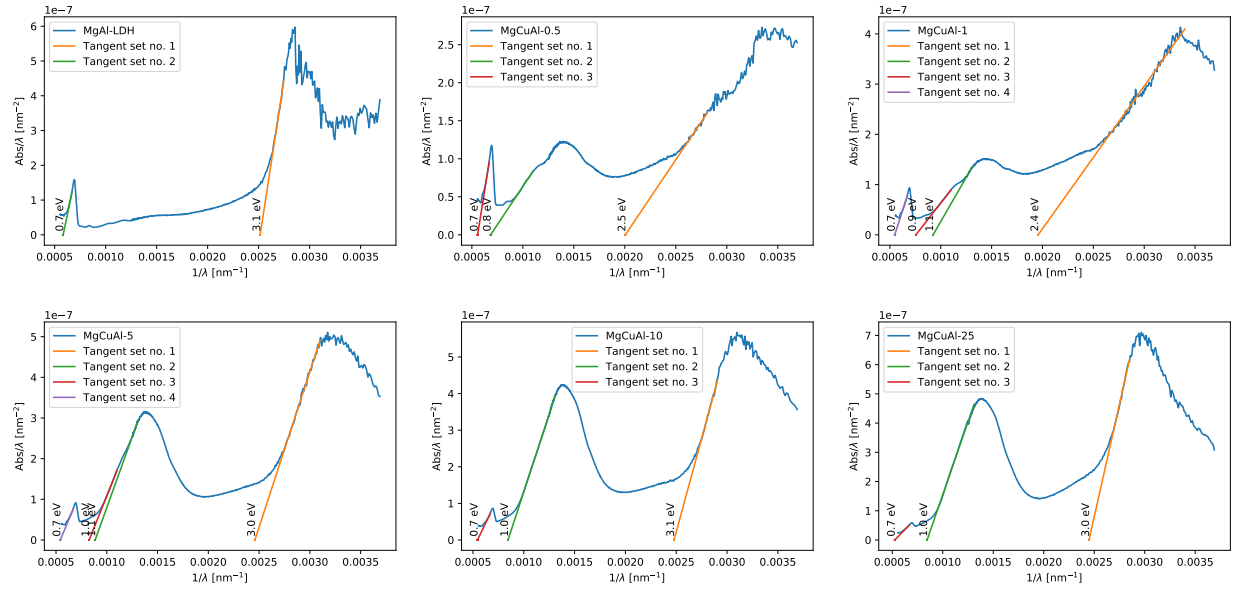

Figure 11 ASF method fitted bandgaps of MgAl-LDH (top left) and the Cu-substituted (0.5, 1, 5, 10, 25% middle left to bottom right) LDHs prepared using CP.

Cu-modification led to the formation of two absorption bands, showing a bandgap of 3.0 eV and 1.0 eV in addition to the typical 0.7 eV near infrared bandgap at 25% Cu-substitution. Doping with 0.5% and 1% yielded lower bandgaps, which increased to their final values from 5% Cu-substitution.

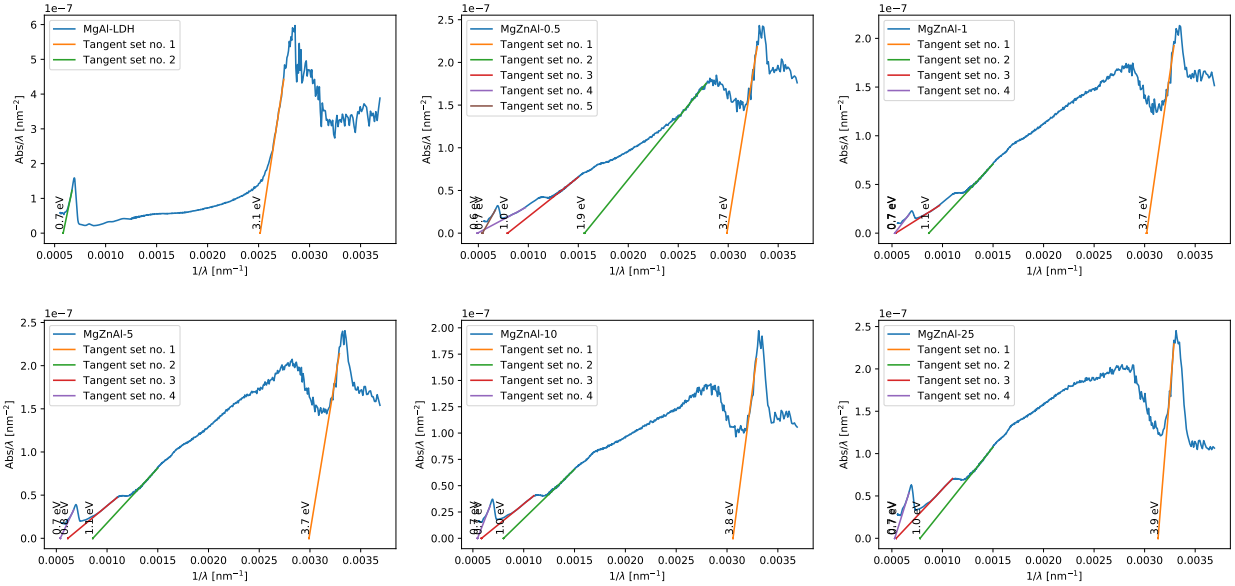

Figure 12 ASF method fitted bandgaps of MgAl-LDH (top left) and the Zn-substituted (0.5, 1, 5, 10, 25% middle left to bottom right) LDHs prepared using CP.

The Zn-modified materials did not show any significant ultra violet or visible light absorbency, but exhibited the typical near infrared absorption band. They all showed a bandgap of around 3.7 eV to 3.9 eV. Lower absorption edges (apart from the 0.7 eV bandgap) were again disregarded because of the low light absorbency.

5.3.2 CoW method

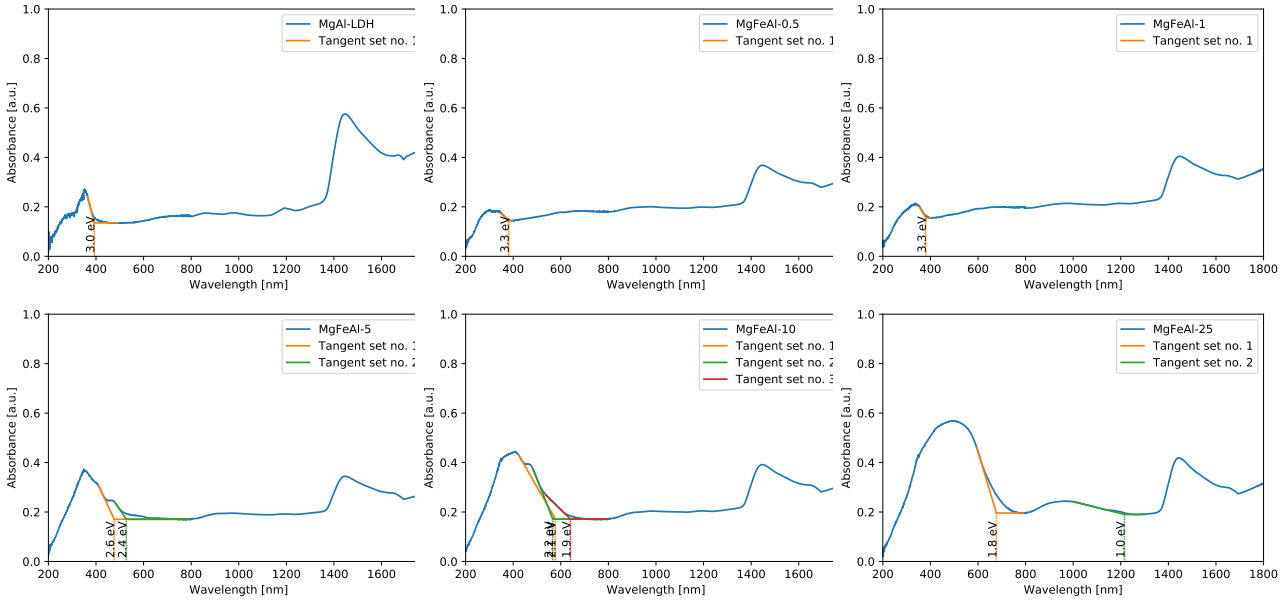

Figure 13 CoW method fitted bandgaps of MgAl-LDH (top left) and the Fe-substituted (0.5, 1, 5, 10, 25% middle left to bottom right) LDHs prepared using CP.

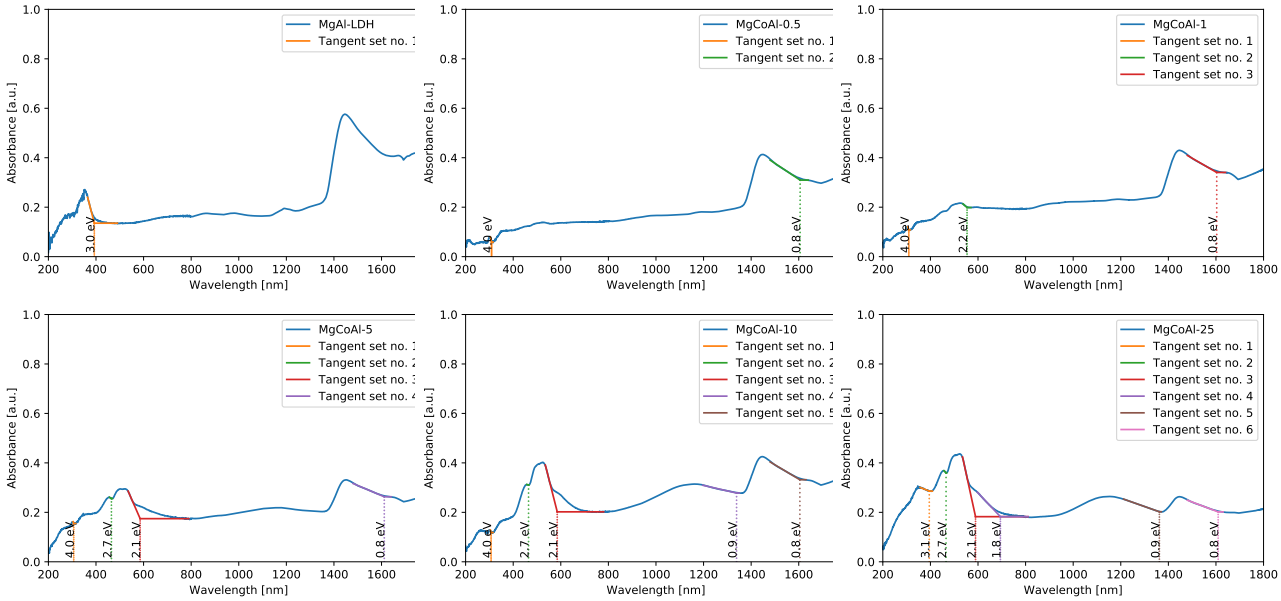

Figure 14 CoW method fitted bandgaps of MgAl-LDH (top left) and the Co-substituted (0.5, 1, 5, 10, 25% middle left to bottom right) LDHs prepared using CP.

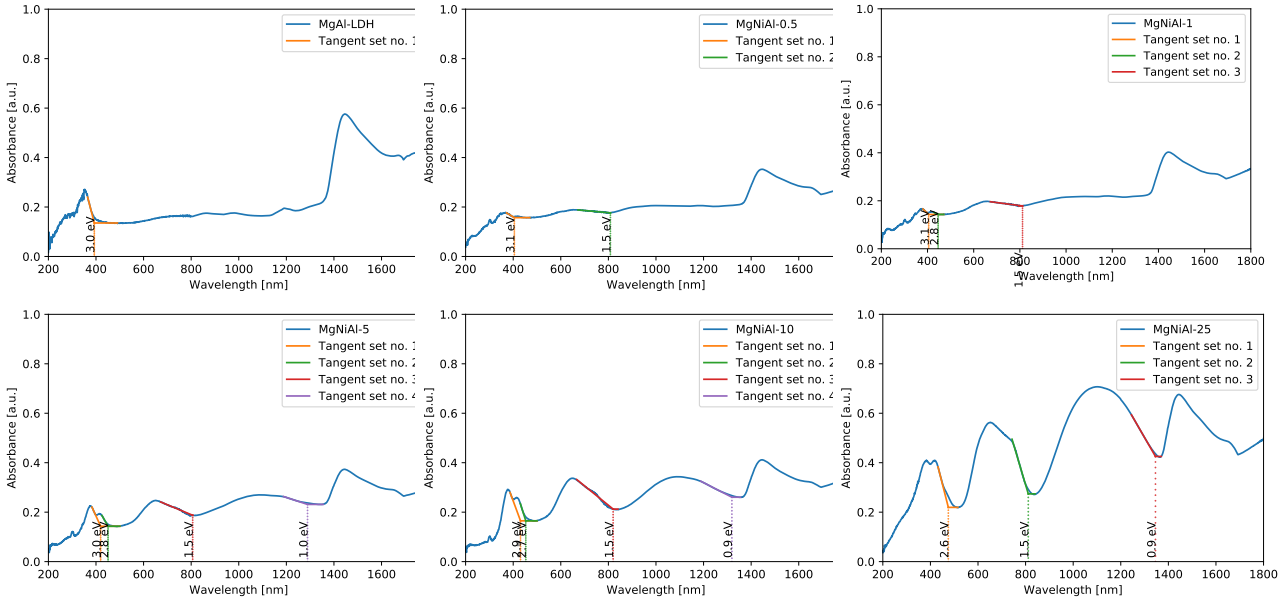

Figure 15 CoW method fitted bandgaps of MgAl-LDH (top left) and the Ni-substituted (0.5, 1, 5, 10, 25% middle left to bottom right) LDHs prepared using CP.

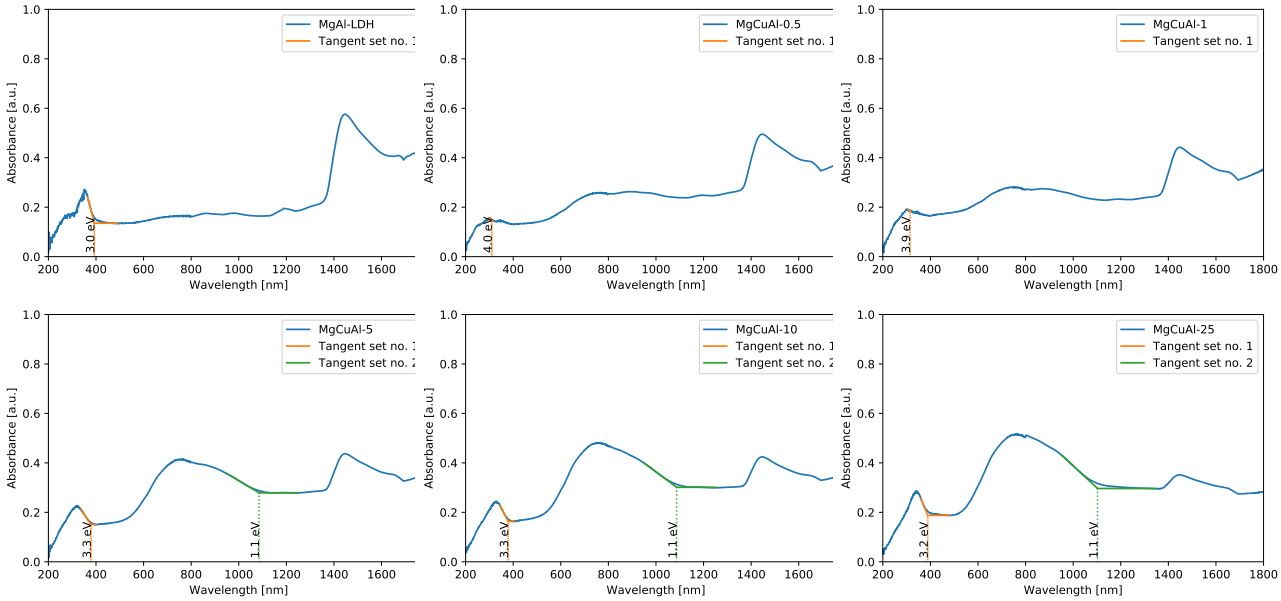

Figure 16 CoW method fitted bandgaps of MgAl-LDH (top left) and the Cu-substituted (0.5, 1, 5, 10, 25% middle left to bottom right) LDHs prepared using CP.

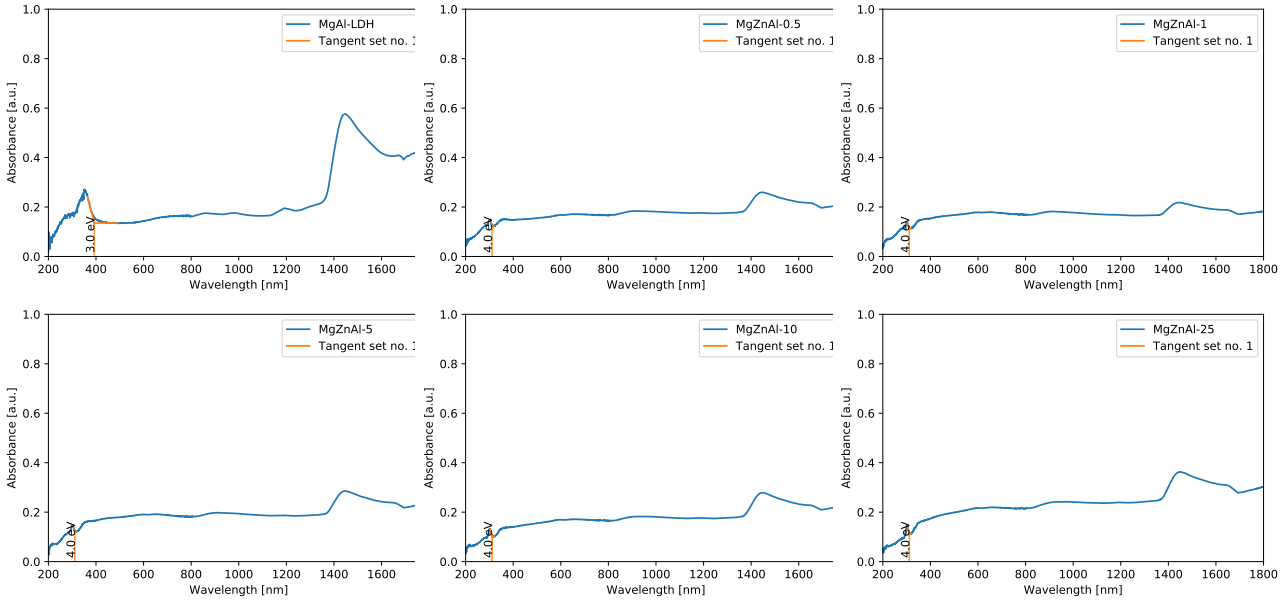

Figure 17 CoW method fitted bandgaps of MgAl-LDH (top left) and the Zn-substituted (0.5, 1, 5, 10, 25% middle left to bottom right) LDHs prepared using CP.

5.3.3 Tauc plot method

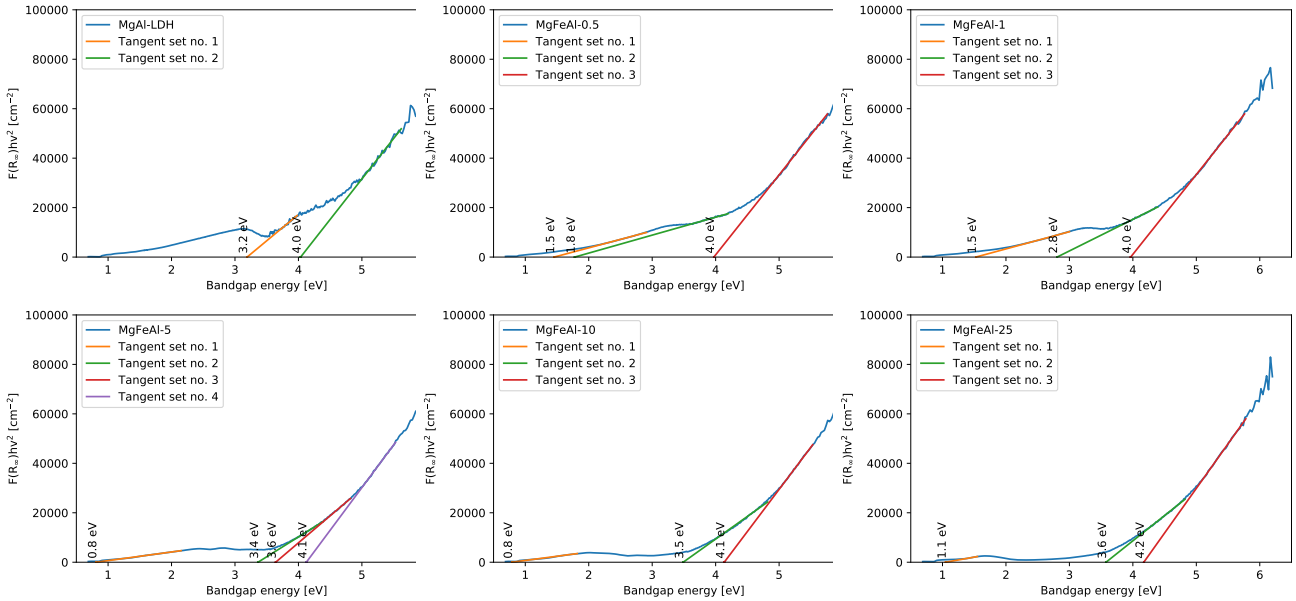

Figure 18 Tauc plot method fitted bandgaps of MgAl-LDH (top left) and the Fe-substituted (0.5, 1, 5, 10, 25% middle left to bottom right) LDHs prepared using CP.

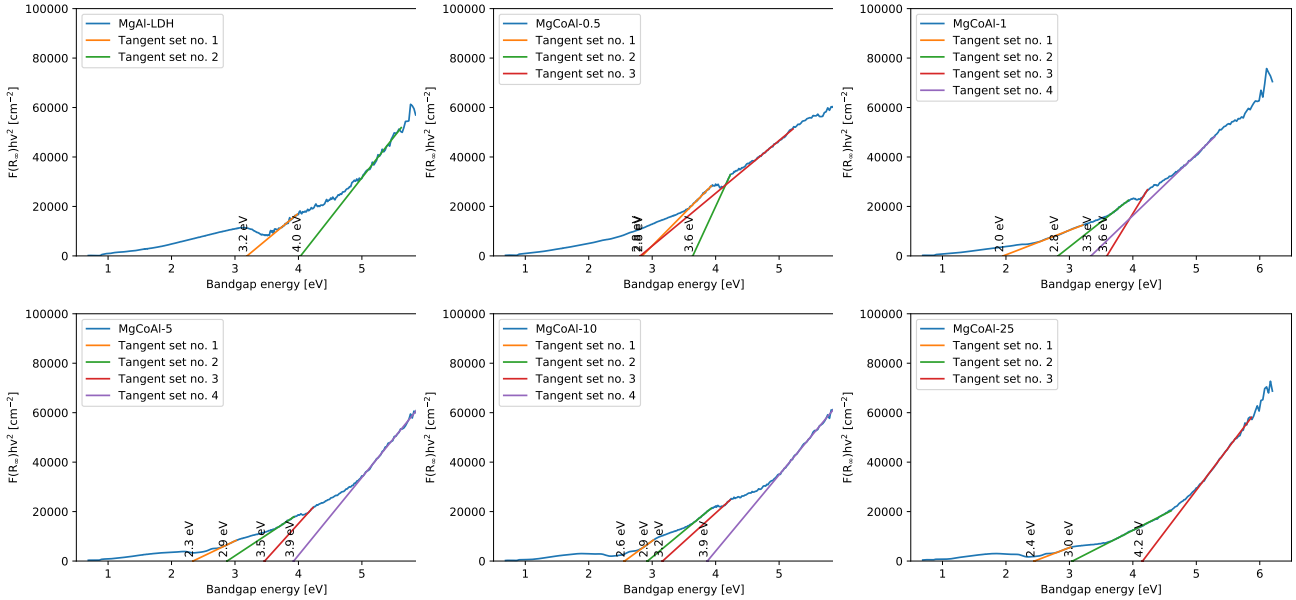

Figure 19 Tauc plot method fitted bandgaps of MgAl-LDH (top left) and the Co-substituted (0.5, 1, 5, 10, 25% middle left to bottom right) LDHs prepared using CP.

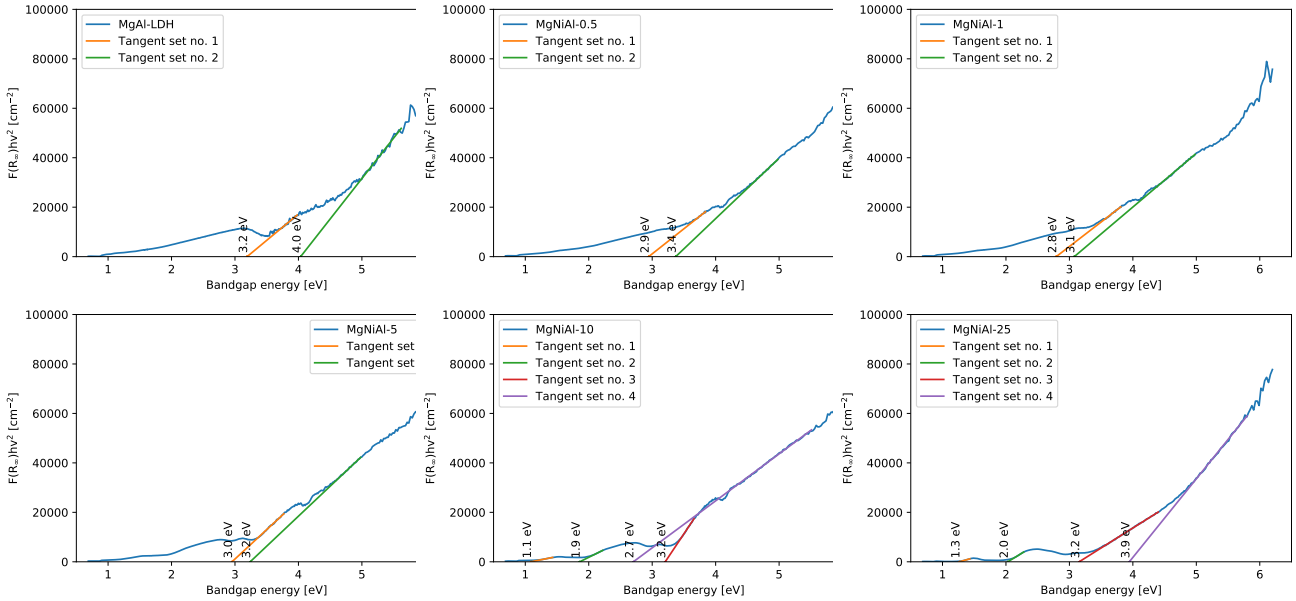

Figure 20 Tauc plot method fitted bandgaps of MgAl-LDH (top left) and the Ni-substituted (0.5, 1, 5, 10, 25% middle left to bottom right) LDHs prepared using CP.

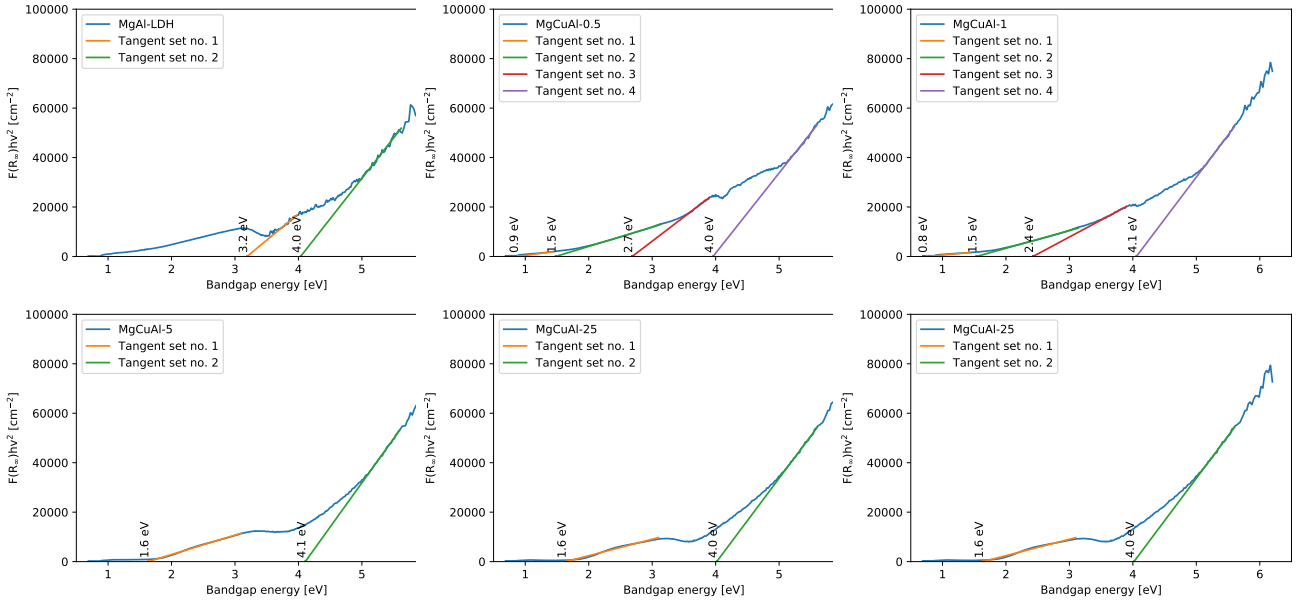

Figure 21 Tauc plot method fitted bandgaps of MgAl-LDH (top left) and the Cu-substituted (0.5, 1, 5, 10, 25% middle left to bottom right) LDHs prepared using CP.

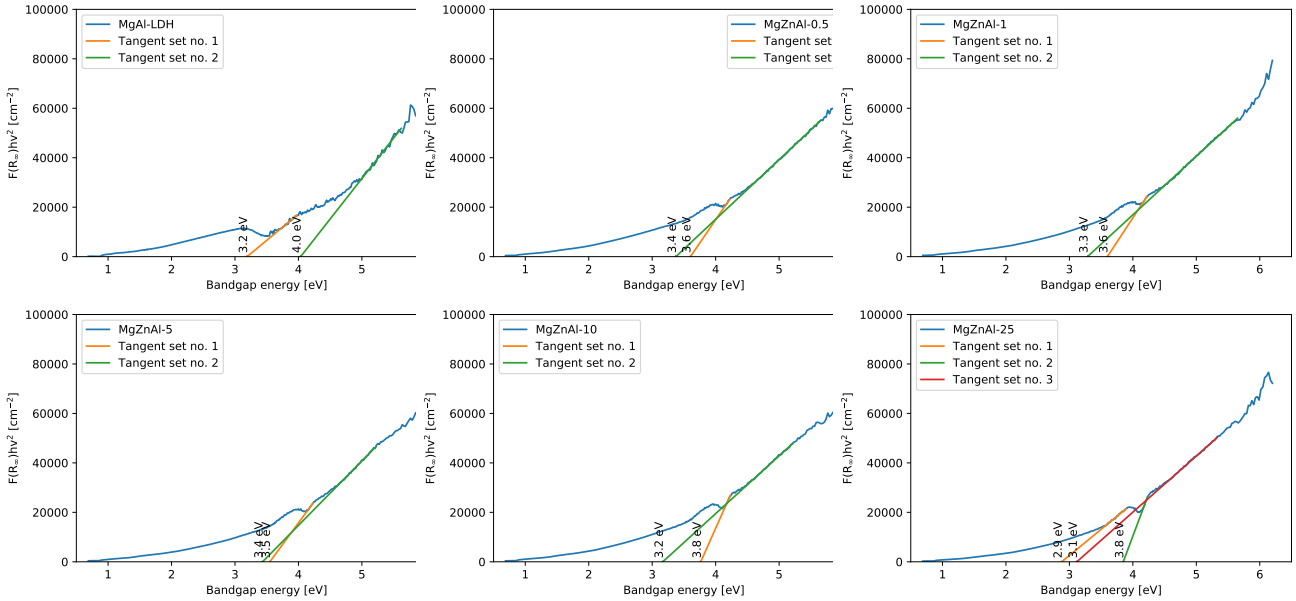

Figure 22 Tauc plot method fitted bandgaps of MgAl-LDH (top left) and the Zn-substituted (0.5, 1, 5, 10, 25% middle left to bottom right) LDHs prepared using CP.

5.3.4 ASF method Urea hydrolysis

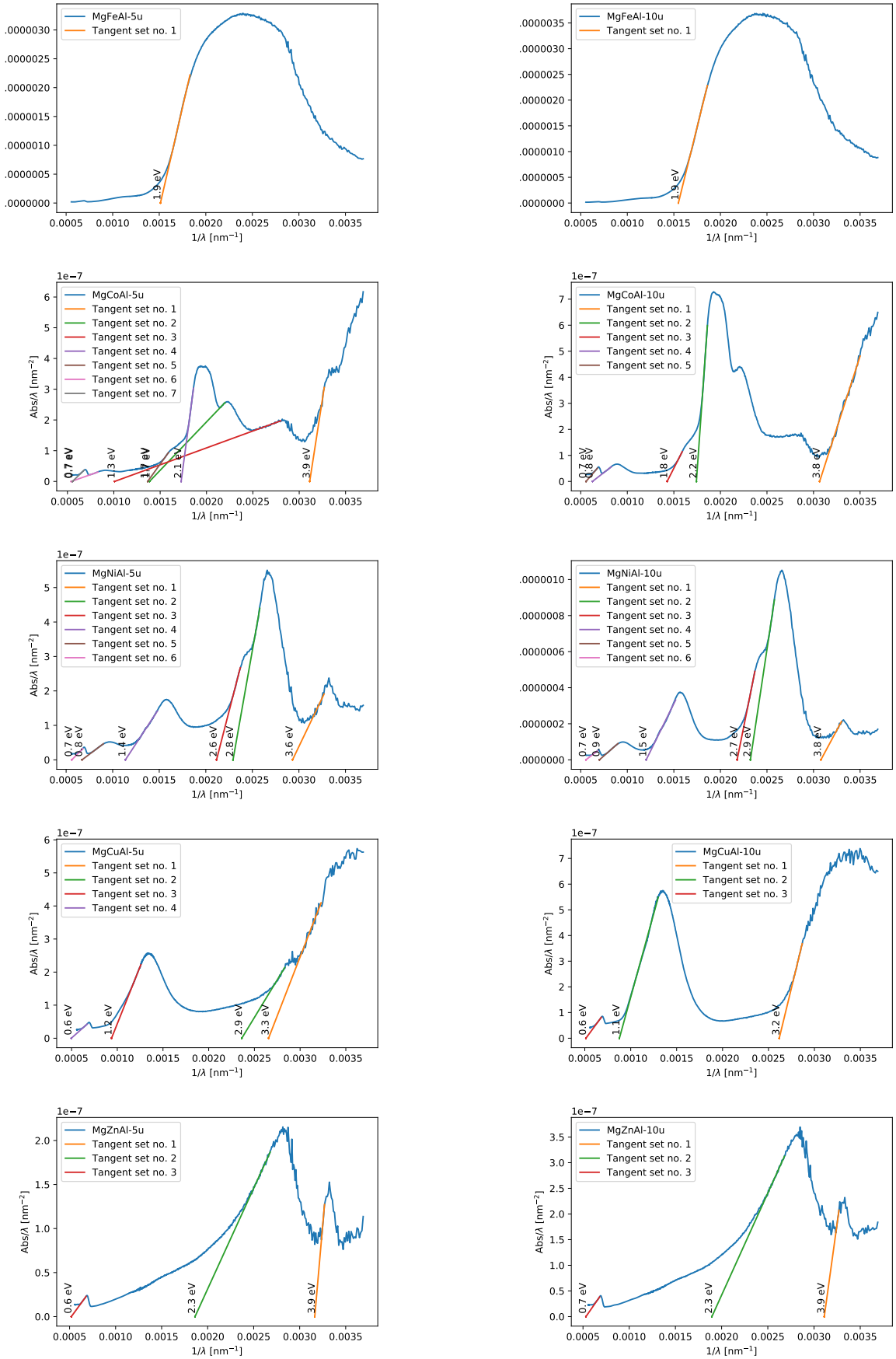

Figure 23 ASF method fitted bandgaps of MgAl-LDH substituted with 5% and 10% of Fe, Co, Ni, Cu and Zn produced using UH.

The spectra obtained for the UH synthesised materials were very similar to those obtained through CP, apart from the Fe-modified MgAl-LDHs, which showed highly increased absorbance. Further, the UH materials showed better absorbance for the Zn-modified materials. For all other materials, the band edges matched those obtained through CP almost perfectly.

6 Full-sized UV-Vis(-NIR) graphs

Figure 24 shows the 0.5% and 1% TM-doped CP LDHs in the UV-Vis range mentioned in the main text. It could clearly be observed that doping the MgAl-LDH with 0.5% and 1% TM led to a reduction in the UV absorption band exhibited by MgAl-LDH. The incorporation of TMs into the lattice, however, led to the formation of additional absorption bands in the case of Fe-, Co-, Ni- and Cu-modification, even for these low TM quantities. All but MgAl-LDH and the Fe-doped LDHs exhibited a small absorption peak at around 300 nm corresponding to around 3.8 eV. This absorption peak, while well visible on this plot, was not easily observed when using the ASF method to determine the band edges of Cu-modified LDH.

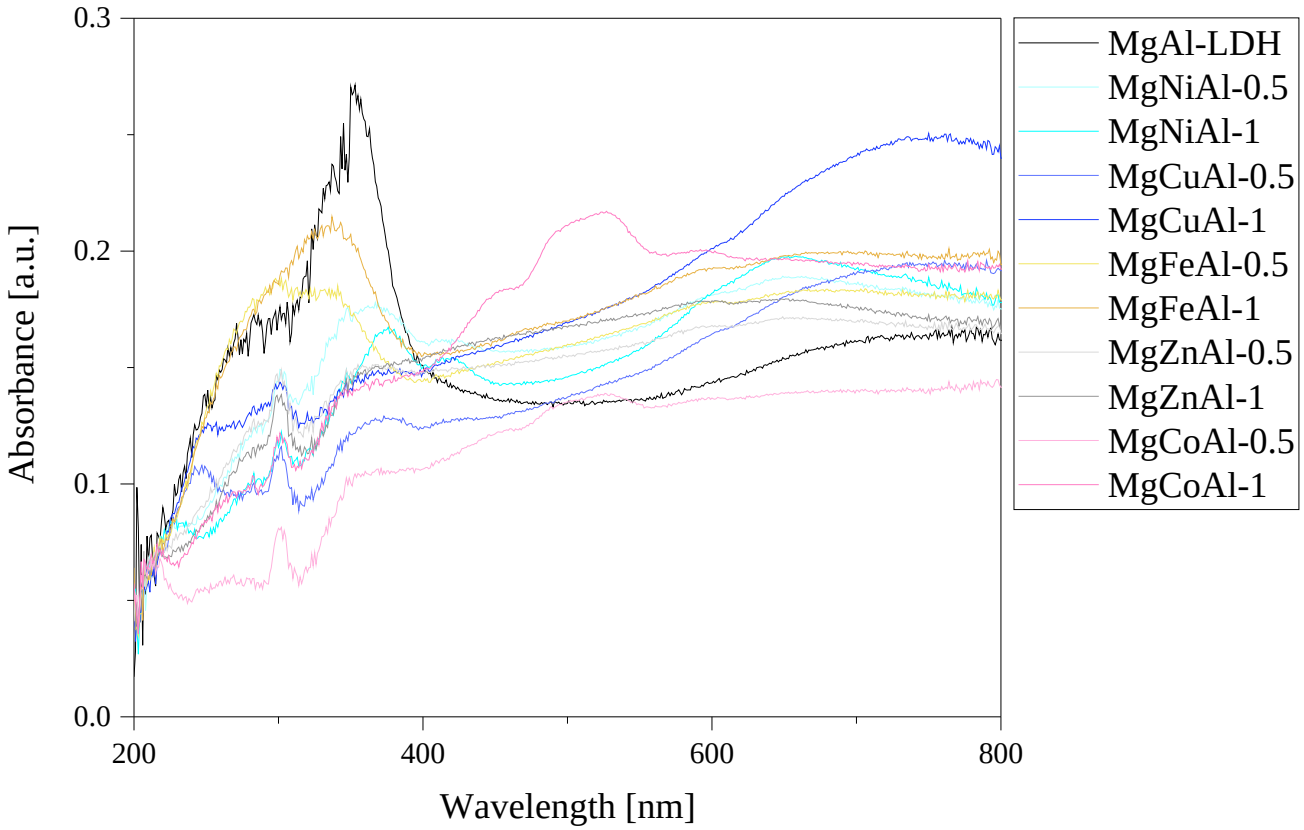

Figure 24 UV-Vis-NIR absorption spectra of MgAl-LDHs prepared using CP with TM-doping of 0.5% and 1% showing the loss of the UV absorbance band upon TM-modification.

Acknowledgements

This research was funded by Techsparks (Pty) Ltd, the Technology and Human Resources for Industry Programme (THRIP) administered by the Department of Trade and Industry, South Africa, (grant number THRIP/133/31/03/2016) and the Leibniz-Institut für Polymerforschung Dresden e.V., Germany. The authors particularly thank David Viljoen for his editing efforts and the supply of software to accurately determine the bandgaps of the materials. Sajid Naseem acknowledges the Higher Education Commission (HEC), Pakistan and the German academic exchange service (DAAD) for his scholarship. Charles J. Sheppard acknowledges funding from UJ-URC and FRC for equipment maintenance.

Notes and references

[1] C. Forano, T. Hibino, F. Leroux and C. Taviot-Guého, *Handbook of Clay Science*, Elsevier, 2006, vol. 1, pp. 1021–1095.

[2] S. Naseem, S. P. Lonkar, A. Leuteritz and F. J. W. J. Labuschagné, *RSC Adv.*, 2018, **8**, 29789–29796.

[3] M. J. Wu, J. Z. Wu, J. Zhang, H. Chen, J. Z. Zhou, G. R. Qian, Z. P. Xu, Z. Du and Q. L. Rao, *Catalysis Science and Technology*, 2018, **8**, 1207–1228.

[4] X. Long, Z. Wang, S. Xiao, Y. An and S. Yang, *Materials Today*, 2016, **19**, 213–226.

[5] Y. Zhao, X. Jia, G. I. Waterhouse, L.-Z. Wu, C.-H. Tung, D. O'Hare and T. Zhang, *Advanced Energy Materials*, 2016, **6**, 1501974.

[6] L. Mohapatra and K. Parida, *Journal of Materials Chemistry A*, 2016, **4**, 10744–10766.

[7] C. Coluccini, I. Sporer, A. Leuteritz, I. Kuehnert and D.-Y. Wang, *Nanomaterials and Energy*, 2014, **3**, 177–191.

[8] J. Li, S. Jiang, M. Shao and M. Wei, *Catalysts*, 2018, **8**, 1–19.

[9] M. Shao, R. Zhang, Z. Li, M. Wei, D. G. Evans and X. Duan, *Chemical Communications*, 2015, **51**, 15880–15893.

[10] W. Shi, M. Wei, D. G. Evans and X. Duan, *Journal of Materials Chemistry*, 2010, **20**, 3901–3909.

[11] G. Prestopino, G. Arrabito, A. Generosi, A. Mattoccia, B. Paci, G. Perez, G. Verona-Rinati and P. G. Medaglia, *Scientific Reports*, 2019, **9**, 1–12.

[12] B. Schwenzer, J. R. Neilson, K. Sivula, C. Woo, J. M. Fréchet and D. E. Morse, *Thin Solid Films*, 2009, **517**, 5722–5727.

[13] Y. Lee, J. H. Choi, H. J. Jeon, K. M. Choi, J. W. Lee and J. K. Kang, *Energy and Environmental Science*, 2011, **4**, 914–920.

[14] R. Nakamura, A. Okamoto, H. Osawa, H. Irie and K. Hashimoto, *Journal of the American Chemical Society*, 2007, **129**, 9596–9597.

[15] H. Yan, M. Wei, J. Ma, D. G. Evans and X. Duan, *Journal of Physical Chemistry A*, 2010, **114**, 7369–7376.

[16] J. S. Valente, F. Tzompantzi, J. Prince, J. G. Cortez and R. Gomez, *Applied Catalysis B: Environmental*, 2009, **90**, 330–338.

[17] S. M. Xu, T. Pan, Y. B. Dou, H. Yan, S. T. Zhang, F. Y. Ning, W. Y. Shi and M. Wei, *Journal of Physical Chemistry C*, 2015, **119**, 18823–18834.

[18] Z. Yang, F. Wang, C. Zhang, G. Zeng, X. Tan, Z. Yu, Y. Zhong, H. Wang and F. Cui, *RSC Advances*, 2016, **6**, 79415–79436.

[19] K. Parida, M. Satpathy and L. Mohapatra, *Journal of Materials Chemistry*, 2012, **22**, 7350–7357.

[20] B. R. Gevers, S. Naseem, A. Leuteritz and F. J. W. J. Labuschagné, *RSC Adv.*, 2019, **9**, 28262–28275.

[21] S. Naseem, B. Gevers, R. Boldt, F. J. Labuschagné and A. Leuteritz, *RSC Advances*, 2019, **9**, 3030–3040.

[22] G. Carja, E. Husanu, C. Gherasim and H. Iovu, *Applied Catalysis B: Environmental*, 2011, **107**, 253–259.

[23] Y. Zhao, B. Li, Q. Wang, W. Gao, C. J. Wang, M. Wei, D. G. Evans, X. Duan and D. O'Hare, *Chemical Science*, 2014, **5**, 951–958.

[24] E. S. Zhitova, S. V. Krivovichev, V. N. Yakovenchuk, G. Y. Ivanyuk, Y. A. Pakhomovsky and J. A. Mikhailova, *Mineralogical Magazine*, 2018, **82**, 329–346.

[25] F. Kovanda, D. Koloušek, Z. Cílová and V. Hulínský, *Applied Clay Science*, 2005, **28**, 101–109.

[26] I. Studenyak, M. Kranj and M. Kurik, *International Journal of Optics and Applications*, 2014, **4**, 76–83.

[27] J. S. Griffith and L. E. Orgel, *Q. Rev. Chem. Soc.*, 1957, **11**, 381–393.

[28] K. D. Warren, *Inorganic Chemistry*, 1974, **13**, 1243–1246.

[29] S. M. Xu, H. Yan and M. Wei, *Journal of Physical Chemistry C*, 2017, **121**, 2683–2695.

[30] V. Rives, *Layered Double Hydroxides: Present and Future*, Nova Science Publishers, 2001, pp. 39–92.

[31] F. Theiss, A. López, R. L. Frost and R. Scholz, *Spectrochimica Acta Part A: Molecular and Biomolecular Spectroscopy*, 2015, **150**, 758 – 764.

[32] F. Cavani, F. Trifirò and A. Vaccari, *Catalysis Today*, 1991, **11**, 173–301.

[33] J. T. Kloprogge, D. Wharton, L. Hickey and R. L. Frost, *Journal of Solid State Chemistry*, 2002, **87**, 623–629.

[34] A. L. Patterson, *Phys. Rev.*, 1939, **56**, 978–982.

[35] Y. Zhao, F. Li, R. Zhang, D. G. Evans and X. Duan, *Chemistry of Materials*, 2002, **14**, 4286–4291.

[36] J. Dharma, A. Pisal and Perkin Elmer, Inc., *Simple Method of Measuring the Band Gap Energy Value of TiO 2 in the Powder Form using a UV / Vis / NIR Spectrometer*, https://www.perkinelmer.com/lab-solutions/resources/docs/APP_UVVISNIRMeasureBandGapEnergyValue.pdf.

[37] J. Tauc, *Materials Research Bulletin*, 1968, **3**, 37–46.

[38] A. R. Zanatta, *Scientific Reports*, 2019, **9**, 11225.

[39] P. Kubelka and F. Munk, *Zeitschrift fuer technische Physik*, 1931, **12**, 593–601.

[40] P. Kubelka, *J. Opt. Soc. Am.*, 1948, **38**, 448–457.

[41] P. Kubelka, *J. Opt. Soc. Am.*, 1954, **44**, 330–335.

[42] J. I. Pankove, *Optical processes in semiconductors*, Dover Publications, Inc., 1975, pp. 34–81.

[43] R. Lu, X. Xu, J. Chang, Y. Zhu, S. Xu and F. Zhang, *Applied Catalysis B: Environmental*, 2012, **111-112**, 389–396.

[44] H. Zazoua, A. Boudjemaa, R. Chebout and K. Bachari, *International Journal of Energy Research*, 2014, **38**, 2010–2018.

[45] E. Dvininov, M. Ignat, P. Barvinschi, M. A. Smithers and E. Popovici, *Journal of Hazardous Materials*, 2010, **177**, 150–158.

[46] N. Sangiorgi, L. Aversa, R. Tatti, R. Verucchi and A. Sanson, *Optical Materials*, 2017, **64**, 18–25.

[47] R. Yamamoto, Y. Moritomo and A. Nakamura, *Physical Review B*, 2000, **61**, 5062–5065.

[48] B. Sujak-Cyrul, B. Kolodka and J. Misiewicz, *Journal of Physics and Chemistry of Solids*, 1982, **43**, 1045–1051.

[49] N. Ghobadi, *International Nano Letters*, 2013, **3**, 2.